LA-4615

c. 3

LOS ALAMOS SCIENTIFIC LABORATORY
of the
University of California
LOS ALAMOS • NEW MEXICO

Measured ^{235}U and ^{238}U Fissioning Neutron Fluence Distributions in the Phoebus 2A Shields: Comparisons with Monte Carlo Calculations

UNITED STATES
ATOMIC ENERGY COMMISSION
CONTRACT W-7405-ENG. 36

Printed in the United States of America. Available from
National Technical Information Service
U. S. Department of Commerce
5285 Port Royal Road
Springfield, Virginia 22151
Price: Printed Copy $3.00; Microfiche $0.95

Written: November 1970
Distributed: March 1971

LA-4615
UC-33, PROPULSION SYSTEMS
AND ENERGY CONVERSION
TID-4500

LOS ALAMOS SCIENTIFIC LABORATORY
of the
University of California
LOS ALAMOS • NEW MEXICO

Measured ^{235}U and ^{238}U Fissioning Neutron Fluence Distributions in the Phoebus 2A Shields: Comparisons with Monte Carlo Calculations

by

Clayton W. Watson

MEASURED ^{235}U AND ^{238}U FISSIONING NEUTRON FLUENCE DISTRIBUTIONS IN THE PHOEBUS 2A SHIELDS: COMPARISONS WITH MONTE CARLO CALCULATIONS

by

Clayton W. Watson

ABSTRACT

Fissioning-fluence distributions for ^{235}U and ^{238}U were measured in the facility and cart shields during the Phoebus 2A reactor tests. These data formed a diagnostic basis for upgrading both the neutron Monte Carlo codes and the Phoebus 2A reactor models being used for Rover neutron environmental calculations at Los Alamos Scientific Laboratory.

Detailed comparisons with corresponding distributions calculated with both initial and improved codes and models are presented. Initial calculations gave results that were in poor to fair agreement with experiment, whereas the improved calculations were generally in good to excellent agreement. The changes required to achieve this agreement are discussed.

Auxiliary studies and data, including calculated fission and absorption-rate distributions throughout a 5000-MW Phoebus 2A reactor-shield system, are presented in appendixes.

INTRODUCTION

The fissioning neutron fluence distributions for ^{235}U and ^{238}U were measured in the shield of the Phoebus 2A reactor, during the 1968 tests, as part of a continuing effort to assess the adequacy of neutron environmental calculations for the Los Alamos Scientific Laboratory (LASL) Rover reactors. These data formed a basis for evaluating the neutron calculational methods (particularly neutron Monte Carlo) and reactor modeling procedures being used at that time. In a follow-up analytical program, these studies led to substantial extension and upgrading of both the neutron Monte Carlo capabilities and the Phoebus 2A calculational models.

Principal results of this work were described previously.[1,2] The present report documents these studies more comprehensively and in considerably more detail. In addition, results of auxiliary studies are given in appendixes.

The Phoebus 2A reactor, designed for 5000 MW at full power, was the largest reactor tested in the Rover nuclear rocket program. During high-power operation the reactor was surrounded by an annular 30-in.-thick aluminum/borated-water facility shield whose dual function was the protection of adjacent test-cell structures from overheating and the depression of test-cell activation levels to permit early reentry after a test series.

The size and internal complexity of this reactor afforded a degree of calculational difficulty that exceeded the capability of the neutron Monte Carlo codes being used at that time, especially for neutron flux calculations in the facility shield. The shield itself was a neutronically simple geometry, which tended to preserve distinctive features in the axial distribution of neutrons incident at its inner surface. These features existed because of large variations, with axial position, in the spectrum and intensity of the Phoebus 2A fast leakage neutrons.

Such variations were produced, in turn, by complexities in the internal construction of the reactor. Thus, the shield provided a convenient structure for measuring neutron distributions from which to infer key characteristics of the neutron transport within the reactor system, particularly in the geometrically complex regions outside either end of the core. These data could then be used diagnostically to assess the adequacy of, and to extend, the calculational tools that had been developed for neutron environmental calculations for the Rover reactors.

Both radial and axial (i.e., parallel with the reactor axis) sample tubes had been built into the Phoebus 2A facility shield for this purpose; fissioning fluence traverses were made in these tubes by irradiating full-length uranium wires during preliminary low-power reactor runs and then measuring the distribution of residual fission-product γ-activity along the wires. Ratios of these activities to those from wires irradiated at the core center were also measured, permitting the results to be normalized to the core center.

REACTOR-SHIELD CONFIGURATION

Except for its larger size and details of its internal design, the Phoebus 2A reactor strongly resembled the Phoebus 1 reactors.[3] Phoebus 2A had an ~ 55-in.-diam graphite/enriched-uranium core, surrounded by an 8-in.-thick beryllium reflector. Reactor control was effected by 18 rotating, full-length cylindrical shells, or "drums" in the reflector, each of which was coated with boron over a 120° sector. Further details of the reactor internal configuration will be presented later in the discussion of calculational models.

Figure 1 shows the reactor approaching the test cell face. The reactor was mounted atop a cart assembly that was made up of a control-actuator and instrumentation hookup room built onto a modified railroad flat car. The roof of this room consisted of a 32-in.-thick aluminum/iron/borated-water shield similar to the facility shield. (The open facility shield is also visible in Fig. 1, at the test-cell face.) The cart shield protected the equipment in the hookup room from radiation damage and also enabled personnel to reenter this area shortly after reactor runs.

For testing, the reactor-cart assembly was positioned at the test-cell face with the cart shield immediately below the facility shield, as shown in Fig. 2. During high-power reactor operation, the shield halves closed around the reactor like a clam-

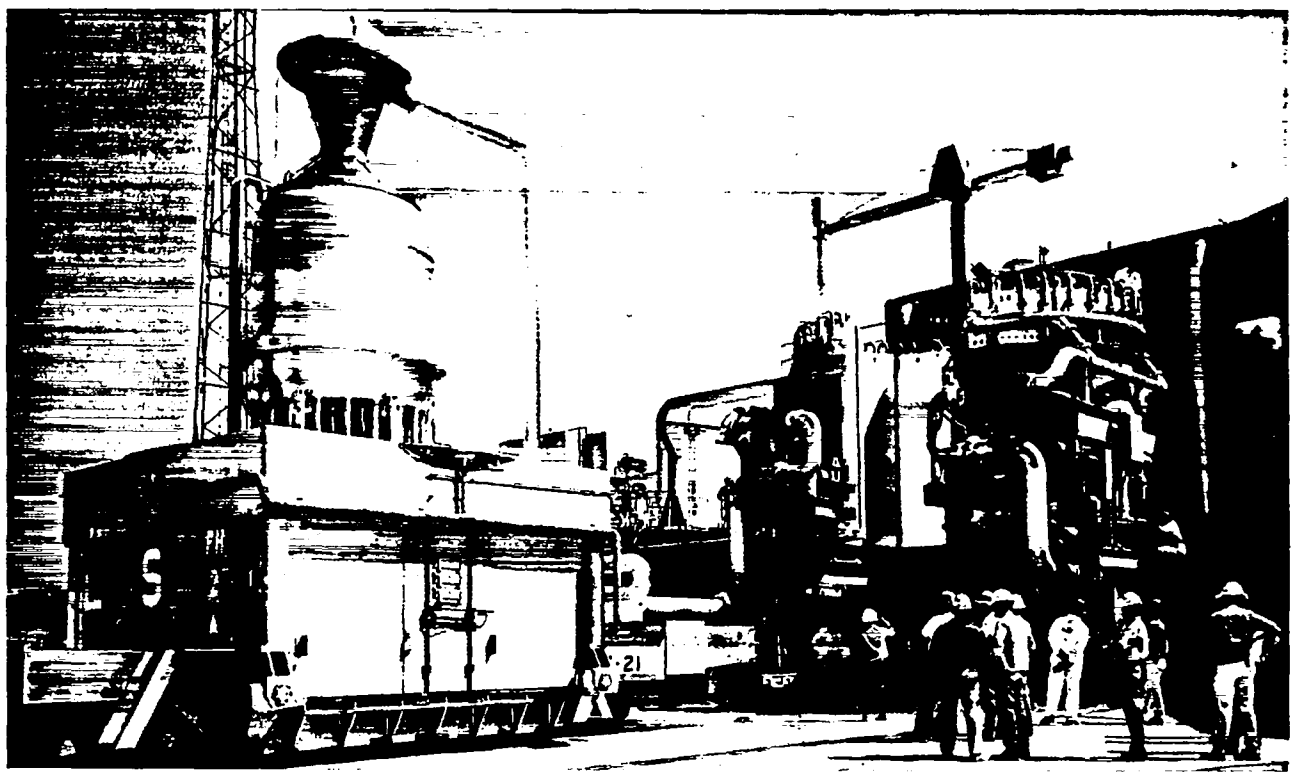

Fig. 1. Phoebus 2A reactor approaching test cell face.

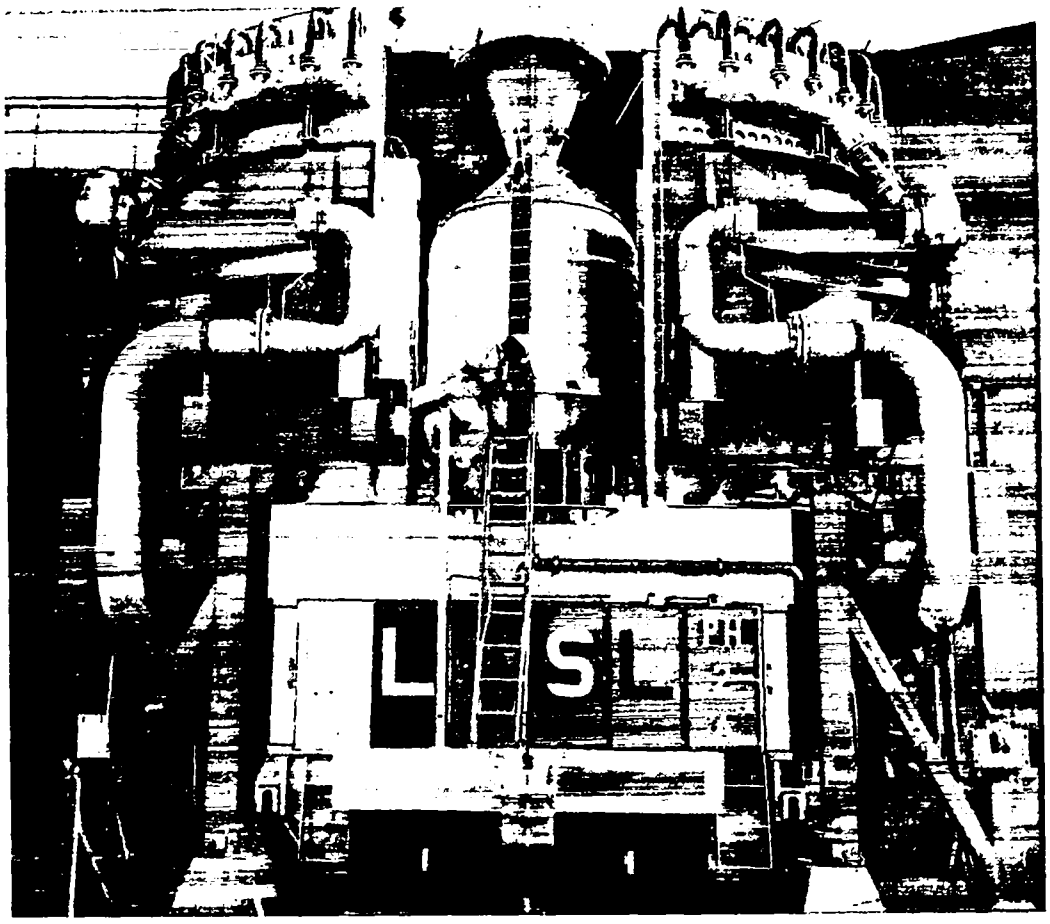

Fig. 2. Phoebus 2A reactor in position for testing, facility shield open.

shell, forming a cylindrical shielding can with the upper end open.

The facility shield consisted of two movable semicylinders, each composed of two close-fitting concentric semiannuli, with four aluminum tanks in each semiannulus, for a total of 16 tanks. The closed shield was 174 in. high, with an o.d. of 169 in. and an i.d. of 107 in. Its overall radial thickness was ~ 31 in.

Portions of a horizontal cross section and a vertical section through the shield are shown in Figs. 3 and 4, respectively. Concentric aluminum plates within each of the tanks formed a multipass flow system through which borated water (~ 2 wt % B) was circulated, as indicated by the arrows in Fig. 4. These plates divided the shield into five radial borated-water regions with thicknesses, inside to outside, of 1.0, 6.5, 4.75, 4.75, and 6.5 in. The radial aluminum thicknesses, inside to outside, were 0.75, 0.25, 0.75, 0.75, 0.75, 2.0, and 0.75 in. The total radial aluminum thickness was 6 in., and that of the borated water was 23.5 in., with an ~ 1.250-in. air gap between the two shield annuli. Locations of 16 radial and eight axial sample tubes are also indicated in the figures. Tubes 1 through 14 were positioned opposite the center of the reactor core. In addition, removable axial sample tubes were temporarily fastened to the inner surface of the shield during the first low-power irradiation.

SHIELD MEASUREMENTS

Wire Fabrication and Emplacement

The ^{235}U measurements were made with 20-mil-diam aluminum wires containing 10 wt % enriched uranium (93.3% ^{235}U). This wire has been used at LASL routinely for several years in reactor flux-distribution measurements.

The ^{238}U wires were specially fabricated for the Phoebus 2A shield measurements. Because of the large thermal-neutron component accompanying the fast-neutron fields that were to be measured,* ^{238}U with

*The maximum expected ^{235}U-to-^{238}U fissioning ratios were several thousand to one.

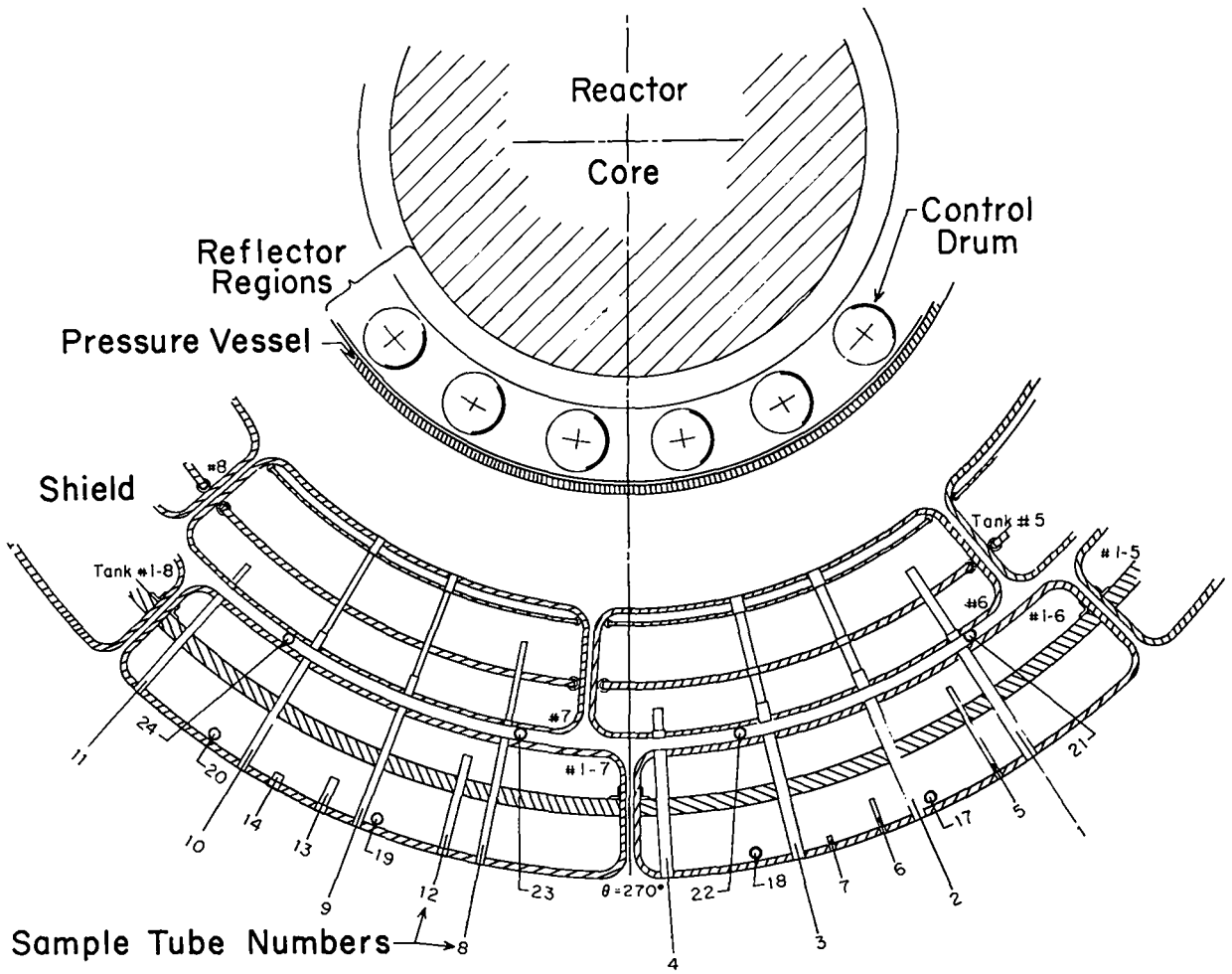

Fig. 3. Partial cross section of Phoebus 2A reactor and facility shield.

very little ^{235}U contamination was required. Approximately 450 g of high-purity ^{238}U oxide, with a ^{235}U content of 2 ppm, were obtained from Oak Ridge National Laboratory (ORNL). This material was reduced to metal and fabricated at LASL into ~ 300 ft of 21-mil-diam wire. Several subsequent analyses and irradiation tests were made in an attempt to verify that the ^{235}U content of the final wire was, indeed, low. Although the verifications were somewhat inconclusive, no evidence of ^{235}U contamination was found. These studies are described in Appendix A.

For the Phoebus 2A irradiations, shield sample tubes were loaded with aluminum and borated-polyethylene inserts to simulate the internal shield structure through which each tube passed. Each insert contained grooves which, after insert assembly, formed four full-length 30-mil-diam holes in each sample tube. The uranium wires were then threaded through these holes.

There were five types of wire placement in the Phoebus 2A shield: (1) 174-in.-long wires were placed axially at the shield inner surface and at radii, from this surface, of 15 and 30 in. (it is estimated that the axial position of these wires was known to within 1 to 2 in.); (2) 30-in.-long wires were placed radially through the shield opposite the core center; (3) 30-in.-long wires were placed radially across the top surface of the shield; (4) 7.5-in.-long wires were placed in coolant channels at the center of the reactor core; and (5) 30-in.-long wires were placed along the axis of the cart shield. Data from the cart wires were not used in the subsequent comparisons, but are presented in Appendix B.

Wire Irradiations

Wires were irradiated during the first two Phoebus 2A reactor tests, designated Experimental Plans 1 and 2 (EP's-1 and -2). Total reactor energy

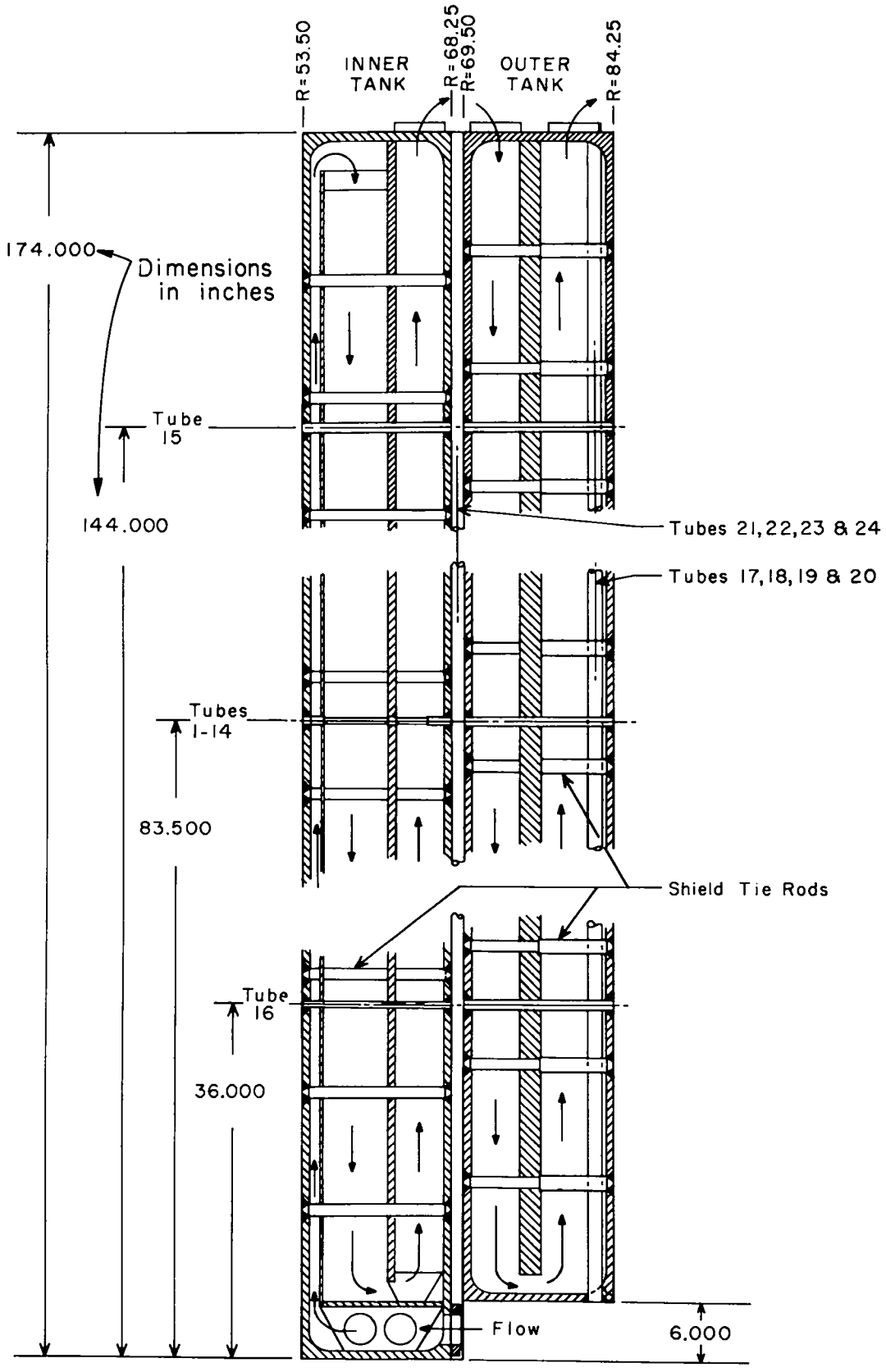

Fig. 4. Vertical cross section of Phoebus 2A facility shield.

TABLE I

PHOEBUS 2A WIRE IRRADIATIONS

	^{235}U Wires						
	Shield, Axial			Shield,	Shield,	Core	Cart,
EP	r=0	r=15 in.	r=30 in.	Radial	Top	Center	Axial
1	yes	yes	no	no	yes	yes	yes
2	no	yes	yes	yes	yes	no	no
			^{238}U Wires				
1	yes	yes[a]	no	no	yes	yes	yes
2	no	yes[a]	no	yes	yes	no	yes

[a]Wires irradiated, but data statistically unusable.

releases during EP-1 and EP-2 were ~ 33 and ~ 1260 MW-sec, respectively. Wires were irradiated as indicated in Table I.

Counting Methods

After irradiation, the wires were returned to LASL and the distribution of residual γ-activity along the length of each was measured by scanning the wire with a NaI(Tl) crystal. (Previous studies had led to choices of 400 and 800 keV, respectively, for ^{235}U and ^{238}U counting biases.) The crystal was a 3 by 3 in. cylinder with a 0.1-in.-diam hole along a diameter through its center.

To reduce background, the crystal was mounted in a cylindrical brass-and-lead shield that also had a diametral hole, aligned with the hole in the crystal. Wires were scanned by pulling them at a fixed rate through the hole in the crystal and reading out total counts accumulated during each of a series of equal, prespecified time intervals. The time intervals typically corresponded to a wire travel of ~ 1 in.; the traversing speeds were adjusted to obtain statistically adequate counting data (typically, 1 to 10% relative error) with reasonable counting times (typically, 5 to 10 min/ft). The overall spatial resolution along the length of a wire was roughly 2 in.

The traversing system consisted of a horizontal, motor-driven, U-shaped yoke with a pin vise on either leg. A wire was inserted by passing it through one pin vise, then through the crystal, then through the other pin vise. As the yoke was driven back and forth, the wire passed through the hole in the crystal. Maximum travel span of the yoke was ~ 26 in.; longer wires were advanced manually by ~ 24 in. after each pass until the entire length was covered. Overall maximum uncertainty of the absolute wire position in the yoke was probably less than ~ 0.5 in. The time, as well as the total counts, A, recorded in each time interval, Δt, were read out periodically by an automatic readout system. (Typically, total counts were recorded during the first 0.5 min out of every 0.6 min, leaving 0.1 min for the readout.) Return of the scanning system to its zero position after each scanning pass, and the initiation of the next pass, were accomplished automatically so as to synchronize each scan with the clock in the readout system.

Data Reduction

The scanning-readout system established a one-to-one correspondence between any two of the following variables:

- t = time after irradiation at which a given counting interval begins.
- Δt = length of the counting interval.
- x = location along the wire of the crystal (or, more exactly, some point of the crystal, e.g., the crystal's edge), at time t.
- Δx = distance that the wire moves during Δt.

Thus, with t, Δt, and A, as recorded by the readout system, plus fission-product γ-decay curves and background counts per unit time, determined separately, the distribution of residual fission-product γ-activity as a function of x can be inferred.

Decay corrections were required to account for the decay of gross fission-product activity during any given wire scan. These corrections were estimated using decay curves measured in the LASL PARKA critical facility,[4] a detailed mockup of the Phoebus 1 reactor. Wires irradiated in PARKA, and counted with the same equipment that was to be used for the Phoebus 2A wires (for biases of both 400 and 800 keV), gave counting rate-vs-time curves from t = 600 min to t = 8250 min after irradiation for ^{235}U and from t = 450 min to t = 5580 min for ^{238}U. The decay time, t, for the Phoebus 2A wires was typically between 700 and 1200 min; the maximum decay correction required for any data point was ~ 25% for some of the low-intensity ^{238}U data, producing an estimated maximum uncertainty of 1 to 2% in the corrected counting rates.

Background corrections were made by periodically counting unirradiated wires identical to the Phoebus

2A wires, and subtracting the resulting counts from the wire-traverse data. Variations in these backgrounds probably constituted the largest uncertainty introduced into the final data, ranging from less than 1% for the ^{235}U data to perhaps 10 to 15% for some of the low-intensity ^{238}U data.

The final axial distributions were plotted as Φ vs Z, where

Z = the distance from the bottom of the shield to the axial position of the center of the given Δx interval,

$\Phi = \phi/\phi_{normalization}$,

ϕ = f(A - background),

f = decay correction,

A = counts recorded during Δt.

Radial data were plotted similarly as Φ vs r, where r is the radial distance from the shield inner surface.

The core-center wires (six ^{235}U and six ^{238}U wires) were counted, averaged, and corrected in the same way.* The ratios of these data to ϕ at the central peak of the axial distributions at the shield inner surface were used to normalize the shield distributions to the core-center values.

Results

Axial distributions at the shield inner surface are plotted in Fig. 5, with the normalization being Φ = 1.0 at the central peak. Representative data points are also shown, indicating the relatively large scatter in the ^{238}U data. To obtain a smoothed

*The counting distribution along these 7.5-in.-long wires was essentially uniform. Thus, count rates measured while the wire was merely centered in the crystal hole could be taken as representative of the entire wire.

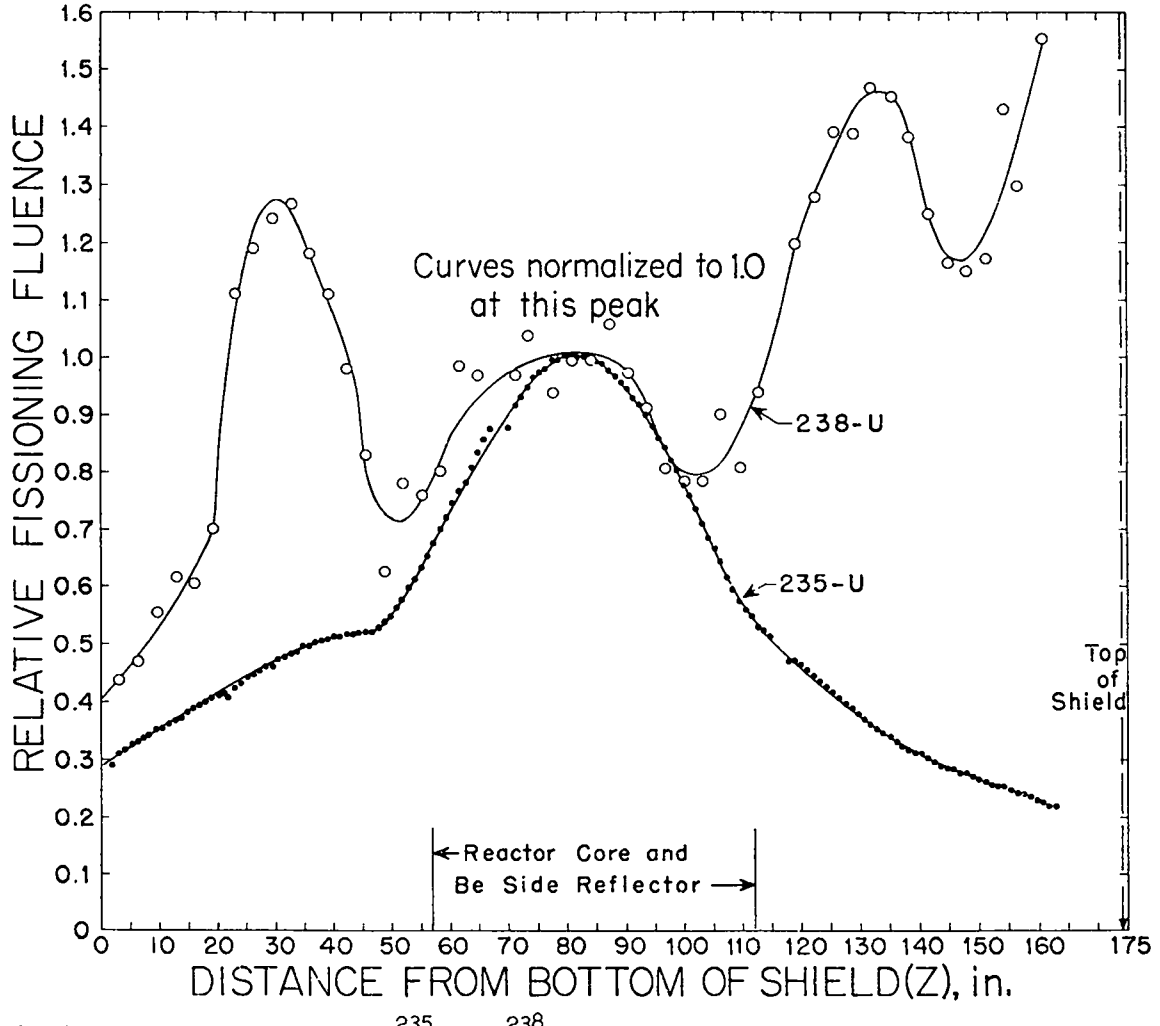

Fig. 5. Axial distributions of ^{235}U and ^{238}U fissioning fluences at shield inner surface.

^{238}U curve, the Z-axis was divided into six intervals, each containing one of the six extrema of Fig. 5, and independent, least-squares, low-order, polynomial curves were fitted to the data in each interval. (The location of the extremum in each interval was also a parameter to be determined in the fitting procedure.) The six resulting curves were then joined smoothly at the ends of the intervals to produce the smoothed ^{238}U curve in Fig. 5. The final maximum uncertainty at any point on the curves in Fig. 5, from all known causes (primarily statistical and background uncertainties), is estimated to be ~ 5% for ^{235}U and 10 to 15% for ^{238}U.

As mentioned earlier, substantial structure is evident in the ^{238}U distribution. The peak at Z ≐ 31 in. is produced by fast neutrons leaking from the core inlet end. In this shield region, the neutrons just miss the inlet end of the reflector and stream through a large aluminum ferrous-metal support structure just above the inlet end of the core. A larger peak at Z ≈ 132 in. is the result of the "plume" of fast neutrons emitted from the core outlet end. This shield region sees the relatively unobstructed end of the core, past the reflector outlet end. These regions will be discussed more explicitly later. There is also a peak in the ^{238}U distribution near the top of the shield, probably caused by reflection of fast neutrons from the surrounding air, or possibly from the test-cell structure.

The ^{235}U distribution has an expected overall shape that is dominated by the leakage of thermalized neutrons through the beryllium side reflector. Here again, however, the shape and magnitude of the ends of the curve (Z = 0 to ~ 55 in., and Z = ~ 115 to 174 in.) are determined by the reactor configurations at either end of the core. Note, for example, the absence of any strongly moderating regions above and below the core.

The measured axial distributions for ^{235}U at 15 and 30 in. from the shield inner surface are plotted in Fig. 6. (The normalizations are arbitrary, and different for the two curves.) At 15 in. into the shield the slow neutrons, all of which entered the shield as fast neutrons, still display a peak at Z ≈ 33 in., but the peak at ~ 132 in. has disappeared. This probably occurs because the relatively unscattered fast neutrons from the outlet-end plume enter the shield at a more glancing angle than those from the reactor inlet end, and suffer a correspondingly greater radial attenuation. A peak at the shield lower end (Z < 20 in.) is produced at r = 15 in. by neutrons streaming through the ~ 3-in.-wide aluminum-and-air gap between the facility shield water and the cart shield water. The corresponding peak at r = 30 in. is obscured by a much larger peak which results from the fact that the outer shield tanks are 6 in. shorter than the inner shield tanks (see Fig. 4).

The sharp peaks at the upper end of the shield are due to the backscattering phenomenon mentioned earlier. The overall curve at r = 30 in. illustrates dramatically the rather local (but adequate) depression of the neutron field that is accomplished by the shield.

Radial data are plotted in Fig. 7, with the normalizations indicated on the figure. The effect of the ~ 3-in.-wide aluminum-and-air gap between the shield annuli can be seen in both the ^{235}U data opposite the core center and in the ^{238}U data across the shield top. The absence of any perturbation in the ^{235}U data across the shield top indicates that these lower-energy neutrons are returning to the shield top from outside the shield, rather than being transmitted axially through the shield structure. Note, also, the flattening of the distributions across the shield top, which is especially marked for the ^{235}U distribution. This is another manifestation of the upper-end axial peaking, or backscattering onto the shield top.

The shield data were normalized to the core center on the basis of (1) the ratio (core center: shield surface opposite the core center), as determined from the core-center data and the axial data at the shield inner surface, and (2) extrapolation to the shield inner surface of the radial curves (Fig. 7) opposite the core center. Unfortunately, both estimates are subject to error. An uncertainty of perhaps 10 to 15% exists in the decay factors required to correct the core-center data to the same decay time as the shield-surface data. These decay factors were large (3 to 5) because the high activity of the core wires meant that they could be counted only after a much longer decay time (t ≐ 3000 min) than the shield wires.

The radial curves in Fig. 7 were extrapolated, with some uncertainty, in three ways: (1) by

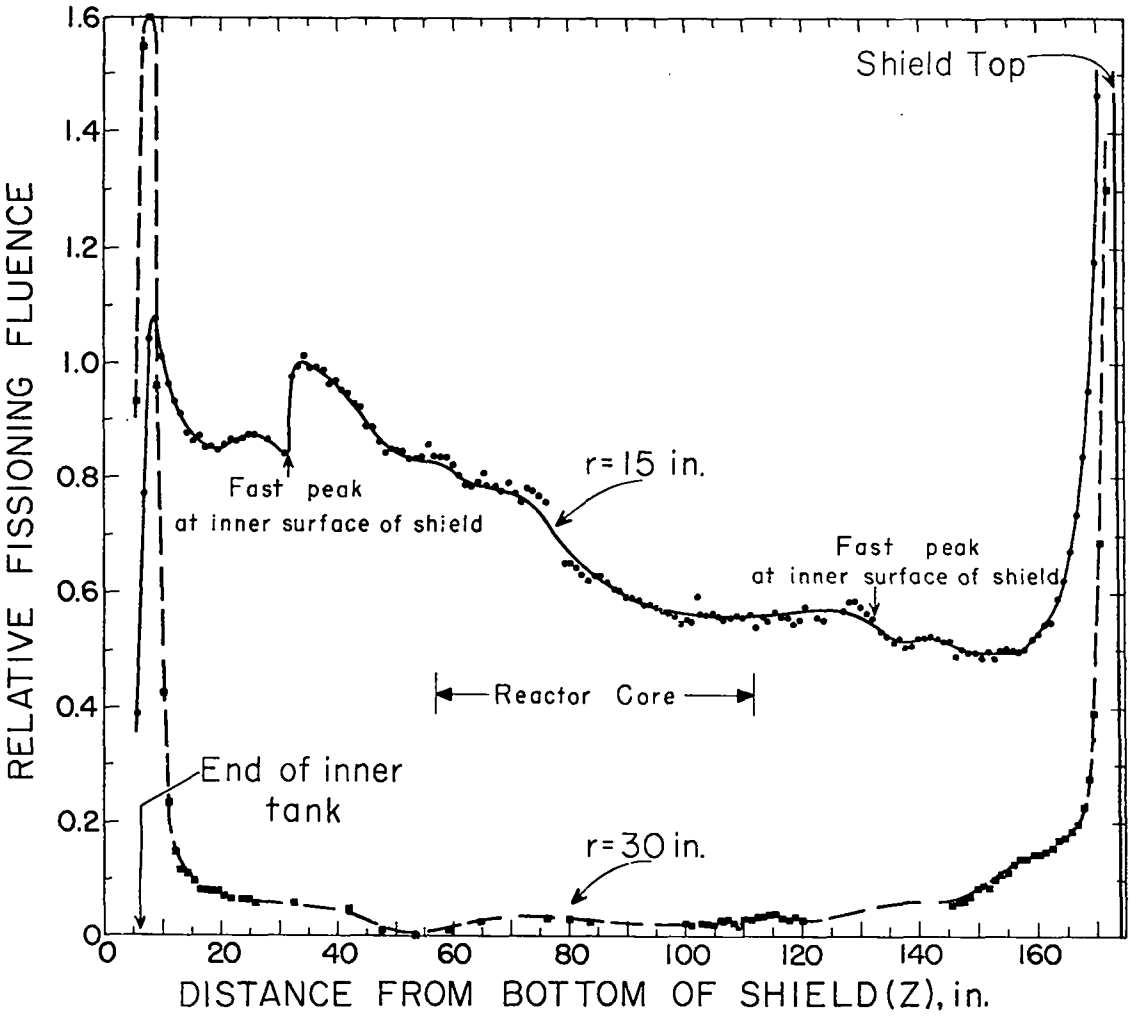

Fig. 6. Axial distributions of ^{235}U fissioning fluence in shield, at r = 15 in. and at r = 30 in.

extrapolating exponential fits to the data in Fig. 7; (2) by using the absolute axial data at the core inner surface; and (3) by radial neutronics calculations (to be described later). On the basis of these results, the values (relative) in Fig. 7 at r = 0 are estimated to be good to within ~ 10%.

Finally, anomalies were discovered in the ^{238}U data for the core center. Although these anomalies proved difficult to assess, subsequent irradiations at LASL indicated that two errors were probably present, and a third is possible. Because of the necessarily long delay after irradiation before the core center wires could be counted, neptunium buildup led to a very intense low-energy (< 500-keV) activity in the wires. This apparently produced crystal fatigue, causing the count rate to decrease by as much as 15% while the ^{238}U wires were being counted. In addition, these low-energy pulses probably piled up in the crystal, causing the ^{238}U counts to be high by a significant, but unknown, amount. Lastly, an unexplained, inconsistent variation with time of the ^{235}U:^{238}U ratio was observed after the irradiations at LASL. This variation may have been a counting-system problem, or it may have been the result of relative differences between the ^{235}U and ^{238}U decay spectra.

The resultant core center-to-shield surface ratios, with roughly estimated uncertainties, are:

For ^{235}U, 5.2 ± (20 to 30%);

For ^{238}U, 480 ± (20 to ? %).

The ratio of the core-center fissioning fluence to that at other points in the shield can be estimated as illustrated in the following example. Estimate the ratio for ^{235}U at the point r = 15 in. and Z = 57 in. (~ opposite the core inlet):

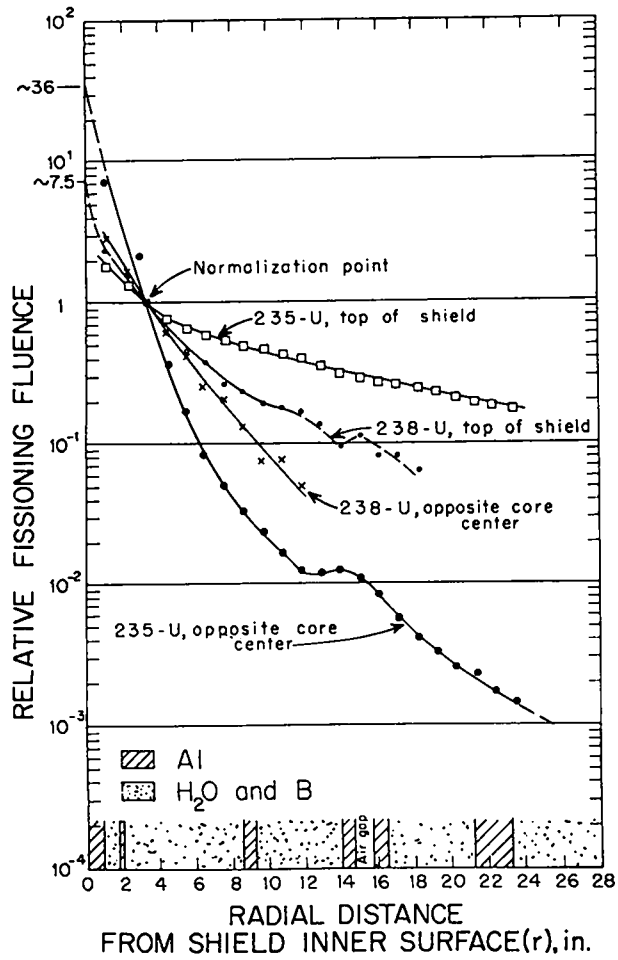

Fig. 7. Radial distributions of ^{235}U and ^{238}U fissioning fluences, through shield opposite core center and across shield top.

From Fig. 6, for r = 15 in.,

$$\frac{\Phi_{57}}{\Phi_{83.5}} = \frac{0.815}{0.620} = 1.315.$$

From Fig. 7, for ^{235}U opposite the core center (Z = 83.5 in.),

$$\frac{\Phi_0}{\Phi_{15}} \doteq \frac{36}{0.0105} = 3430.$$

Also, $\Phi_{\text{core center}}/\Phi_{\text{shield surface}} \doteq 5.2.$

Thus,

$$\Phi_{\text{core center}}/\Phi_{r=15,z=57} \doteq (5.2)(3430)(1.315) = 23{,}450.$$

In an auxiliary series of measurements made ~ 500 days after the Phoebus 2A tests, aluminum samples were taken from the inner surface of the facility shield, from across the top of the facility shield, and from across the top surface of the cart shield. The residual ^{65}Zn γ-activity in these samples was counted to give estimates of the neutron-absorption distributions in the aluminum from the Phoebus 2A tests. These data are presented in Appendix C.

CALCULATIONS AND COMPARISONS

Introduction

The remaining sections describe a follow-up analytical effort, with emphasis upon the changes that were required in the Monte Carlo codes and in the reactor model to obtain agreement between calculation and experiment.

Initial Calculations

In the first phase of the calculations, an existing code was used with a reactor model that had been prepared previously for criticality calculations. This model was known to be too crude and incomplete for calculating external fluxes, and the goal was to examine the character of the disagreement produced by these known deficiencies.

Neutron environmental problems for the previous Rover reactors stemmed primarily from fast-neutron effects, such as direct neutron heat deposition, and the existing Monte Carlo code had been developed primarily for such fast-neutron calculations. (Actually, a series of slightly different, but closely related, codes is implied whenever the word "code" is used. These reflect different stages in the code evolvement process, as well as differences in detail that depend upon the particular problems being studied.) The code was based upon an earlier LASL Monte Carlo Code,[5,6] and can be qualitatively described as follows:

> Any three-dimensional, time-independent geometry made up of first- and second-degree surfaces can be treated.
>
> Relatively standard variance-reducing techniques are included, e.g., importance sampling for energy and spatial distributions of the source, plus path-length "stretching," splitting, and Russian Roulette as a function of position.
>
> Detailed microscopic cross sections are used, with emphasis upon realism in the reaction physics, even at the expense of computing time.
>
> No genuine thermalization routine is included; below a prespecified energy, E_{th}, isotropic scattering from stationary nuclei is assumed, with constant energy and cross sections. (Much of the cross section library, from Lawrence Radiation Laboratory and LASL, was

originally designed for fast-neutron calculations, so low-energy detail is lacking.)

Tallies include fluxes and currents at any surface, plus cell-wise tabulations of absorptions, fissions, elastic-scattering energy deposition, and fission cross-section-weighted total path lengths. The path-length tabulations[3] can be compared directly with the measured fissioning fluences.

Figure 8 shows the original reactor model and the Phoebus 2A shield configuration that was added. This reactor model included those internal details that were significant from the standpoint of criticality calculations, but lacked extra-core features of significance in determining external neutron fluences, e.g., detail was lacking in the inlet-end support, plenum, and pressure-vessel dome regions, as well as in the drum-drive, side-support, and pressure-vessel flange areas. Also, nozzle, nozzle-support, and nozzle-closure regions were not included.

The reflector and control drums had been mocked up in considerable detail (Fig. 9), because they were among the principal areas of interest in the criticality calculations. The three-dimensional character of the control drums also was expected to be significant in determining the external thermal-neutron distributions.

Results of calculations with this code and model are compared in Fig. 10 with the measured ^{235}U axial distribution at the shield inner surface. Here, as in all such comparisons, the measured curve was integrated over spatial intervals identical to those in the Monte Carlo calculations, to give the solid histogram. The calculated histogram was then fitted (or normalized), in a least-squares sense, to the measured histogram, giving the dotted lines in the figure. Superficially, the comparison in Fig. 10 is good. However, there are important discrepancies. The calculated shape is too flat, which implies a poor calculation of the thermalization and attenuation of slow neutrons off the ends of the core, e.g., in the support-plate and nozzle regions. Further, calculated ratios to the core center did not agree at all well with the measured values, and the radial comparisons opposite the core center (not shown) were in only fair agreement with experiment, indicating an inadequate thermalization treatment in the shield.

Even greater discrepancies were present in the ^{238}U axial data, as seen in Fig. 11. Although the ^{238}U experimental errors are larger than those for ^{235}U, the fast-neutron calculations were expected to be relatively good. Because, clearly, the calculations fail badly to reproduce the distinctive shape of the ^{238}U curve, a sensitivity of the external fast-neutron fields to the aforementioned reactor model details was indicated, e.g., the height of the peak at ~ 132 in. is undoubtedly sensitive to the nozzle structures.

Further analysis of these calculated results indicated that considerably more detail and geometrical realism were required in many areas of the reactor model, and that the thermalization routine in the Monte Carlo code needed substantial improvement. Also, new cross-section evaluations with increased resolution at lower energies were available for incorporation into the Monte Carlo library.

New Code and Reactor Model

For the above reasons it was decided to overhaul completely both the code and the reactor model, and to determine how closely the experimental data could be reproduced if the known deficiencies were corrected. Three ground rules were assumed: (1) The Monte Carlo thermalization routine and the Monte Carlo cross-section library were to be updated, with the general goal of dealing more adequately with neutron thermalization in complex moderating geometries. (2) A detailed new physical model of the Phoebus 2A reactor was to be prepared with the goal of calculating external neutron fields rather than criticality. (3) No quantitative inputs from the measurements were to be used to determine the design of either the new code or, more importantly, the new reactor models; i.e., the data were to be ignored except for the above-mentioned qualitative indications as to why bad agreement had been achieved with the earlier calculations. In other words, the result was to be an assessment of the adequacy of an updated but unbiased calculation, i.e., a test of current ability to calculate the Phoebus 2A reactor-shield system as if the reactor were yet to be run, given only the knowledge that considerable improvement over the earlier calculations was needed.

An updated cross-section library tape was prepared which included several new and more detailed evaluations from LASL and from Aldermaston (U.K.). The increased energy resolution of these data raised

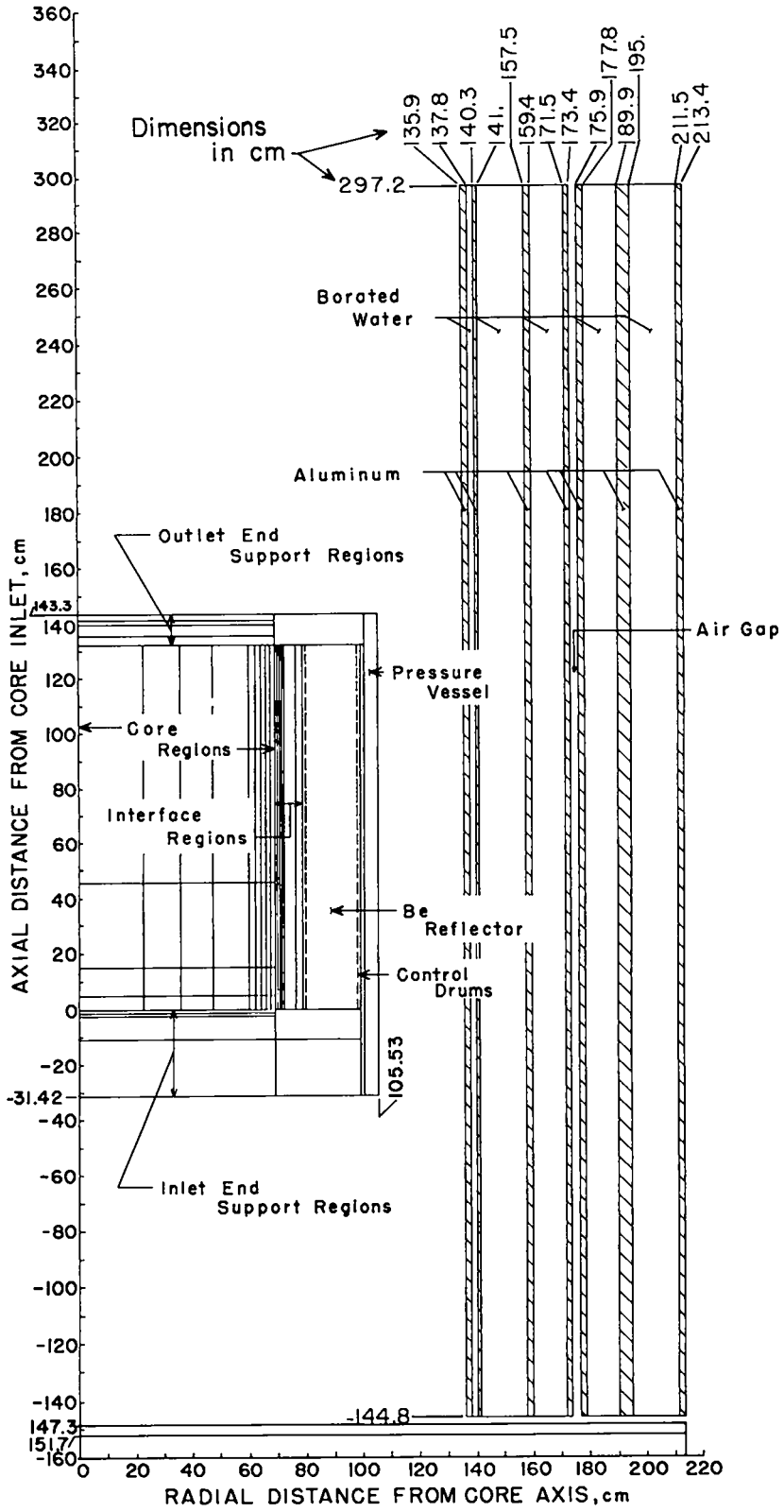

Fig. 8. Initial calculational model, reactor with added facility shield.

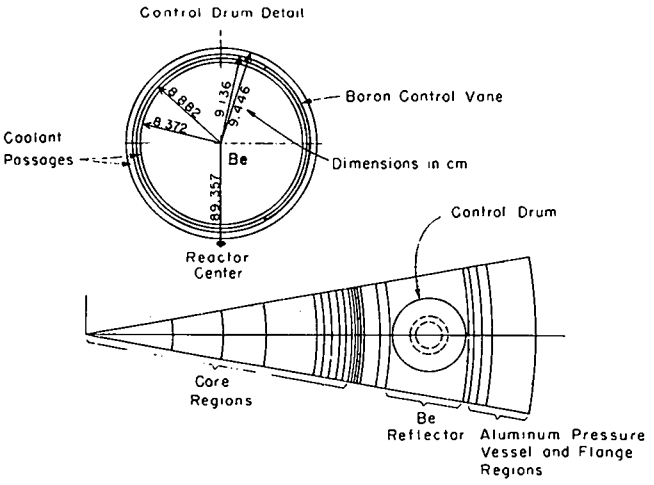

Fig. 9. Initial calculational model, control drum detail.

the library storage requirements for the Phoebus 2A calculations from ~ 6000 to ~ 26,000 words. Since the existing Monte Carlo code was written in the FLOCO language[6] for the 32,000-word IBM-7094, the increased storage requirement, plus other needed code changes, prompted the complete rewriting of the code in FORTRAN for the CDC-6600 computer (~ 130,000 words of fast storage).

The new code contains several improvements in calculational efficiency and includes new input formats that facilitate setting up complex problems. More important, a new "free-gas" thermalization routine had been developed,[7,8] and a modification of this routine was added. In the modified routine, collisions below a presepcified energy, E_t, are elastic collisions with moving target nuclei, assumed to be moving with a Maxwellian distribution of velocities at an input temperature, T. Target nuclei have mass M, and the scattering cross section is σ_t. Both M and σ_t are input parameters and may be specified as a function of energy over the thermal range.

A new reactor model was also prepared from detailed drawings of the Phoebus 2A system and from careful tabulations of the materials and weights in each region. The new model is shown in Figs. 12 through 14. (The reflector, control-drum, and shield models were the same as in Figs. 8 and 9.) Dimensions, in cm, are indicated in the figures for each material region; the circled numbers correspond to the material specifications given in Table II. Several previously mentioned features have been added: inlet-end details such as flow diverters and structural components, pressure-vessel details such as flanges, pressure-vessel dome details, drum actuating mechanisms, nozzle, nozzle inlet torus, nozzle pressure-vessel closure, and nozzle support. Most of these components are metallic structures that may be expected to affect the external neutron fields.

Final Calculations

Three types of problems were run with the new code and new model: (1) a complete calculation with the control drums at 90° (as in Fig. 9); (2) a repeat of the first problem with the drums at 120°, to determine whether external fluxes were sensitive to drum position; and (3) continuations of each of these two problems with a cutoff energy of 0.1 MeV, to decrease the statistical errors of the ^{238}U results. Total size of each of these problems was ~ 65,000 words. Running times were ~ 8 h each (~ 25,000 histories) for problems (1) and (2), and an additional ~ 5 h (each) (~ 125,000 histories) for problems (3).

An isotropic fission-neutron source was used, with axial and radial distributions as shown in Figs. 15 and 16. Tallies included fissioning fluences (weighted path-length tabulations), absorptions, and fissions, for each cell, and currents and fluxes for selected surfaces. Deposition cells, cell volumes, and calculated results other than the fissioning fluences are given in Appendix D.

No statistically significant differences were observed in the shield results for the two different control-drum positions. However, differences were evident in some reactor internal absorption rates and in the fission peaking at the core edge (see Appendix D). For the following comparisons, therefore, the shield data from all runs were combined.

Figure 17 compares the measured and calculated ^{235}U axial fissioning-fluence distributions at the shield inner surface. Agreement here is excellent. Both the relative errors for the Monte Carlo results and the estimated uncertainty of the measured data are ~ 5%. The agreement is within this uncertainty for all intervals in Fig. 17.

A similar comparison for ^{238}U is given in Fig. 18. The estimated error bars (one standard deviation) are also included for each interval. Agreement here, although far from perfect, is still good, and much better than that for the initial calculations.

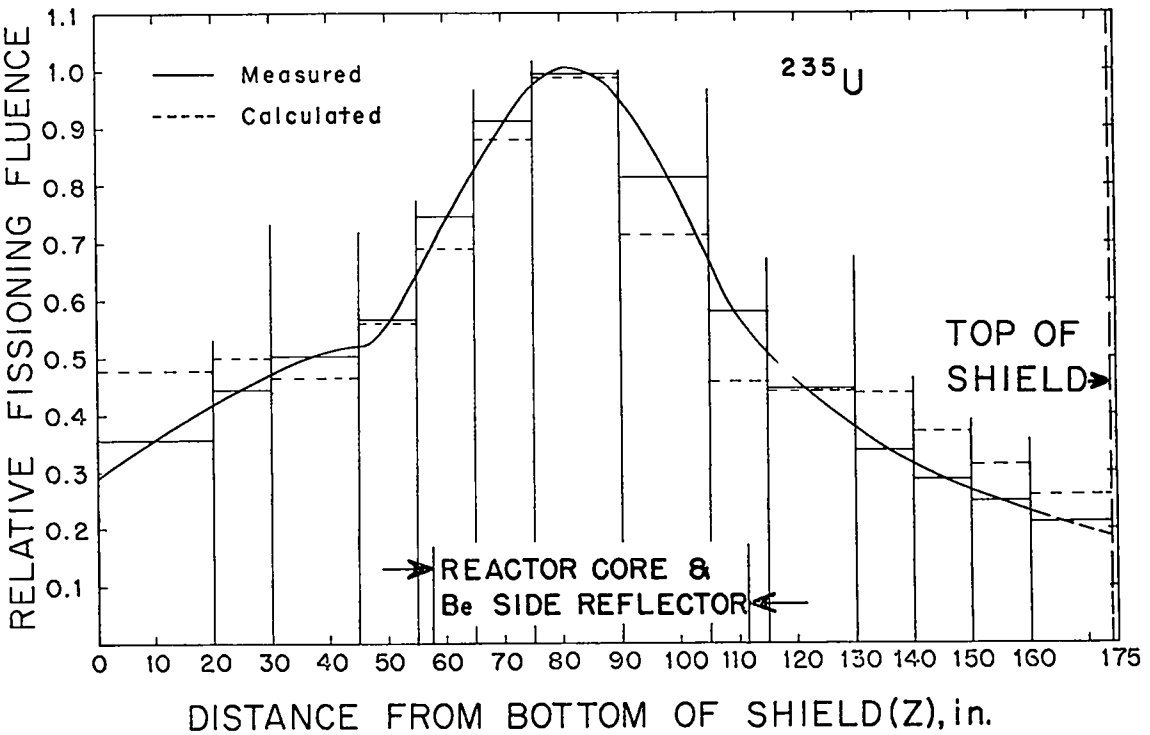

Fig. 10. Comparison of initial calculations with experiment, ^{235}U axial distribution at shield inner surface.

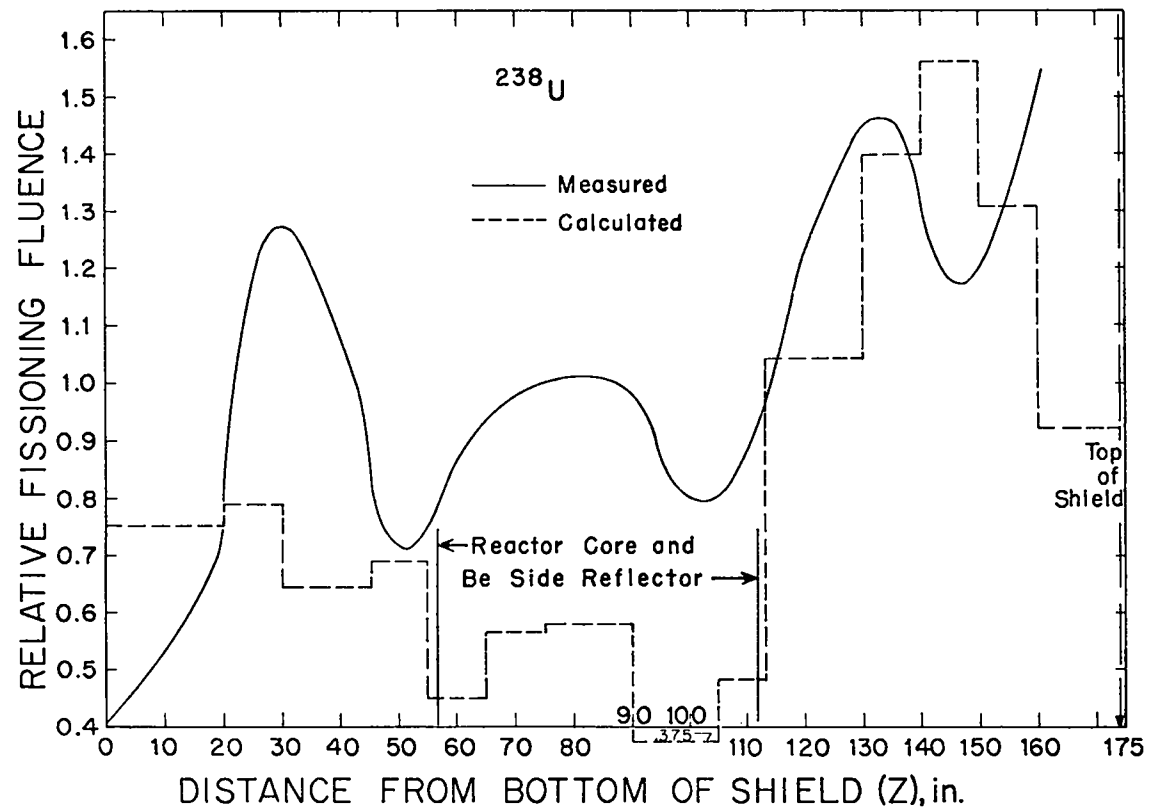

Fig. 11. Comparison of initial calculations with experiment, ^{238}U axial distribution at shield inner surface.

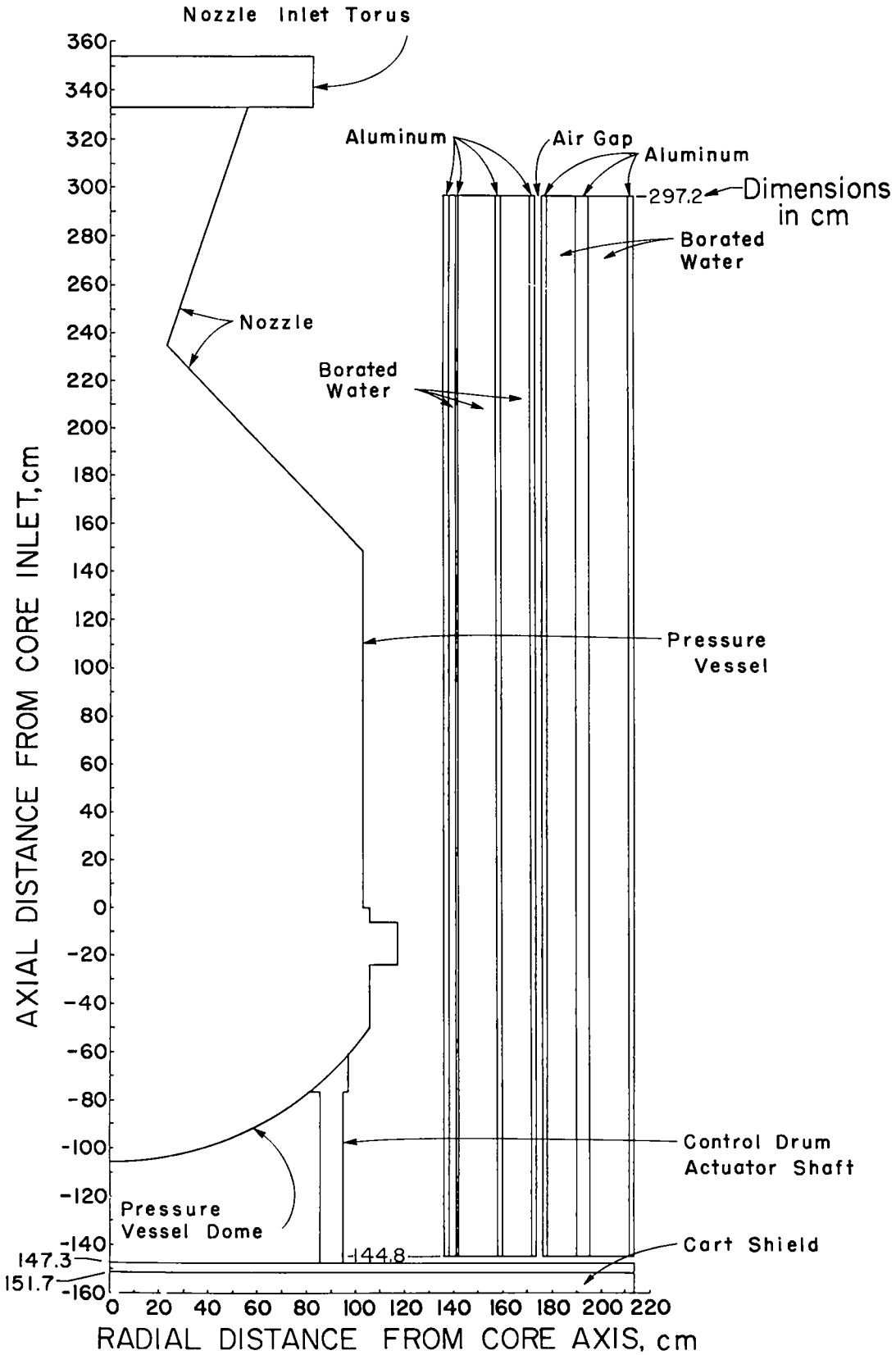

Fig. 12. Final calculational model, reactor outline plus cart and facility shields.

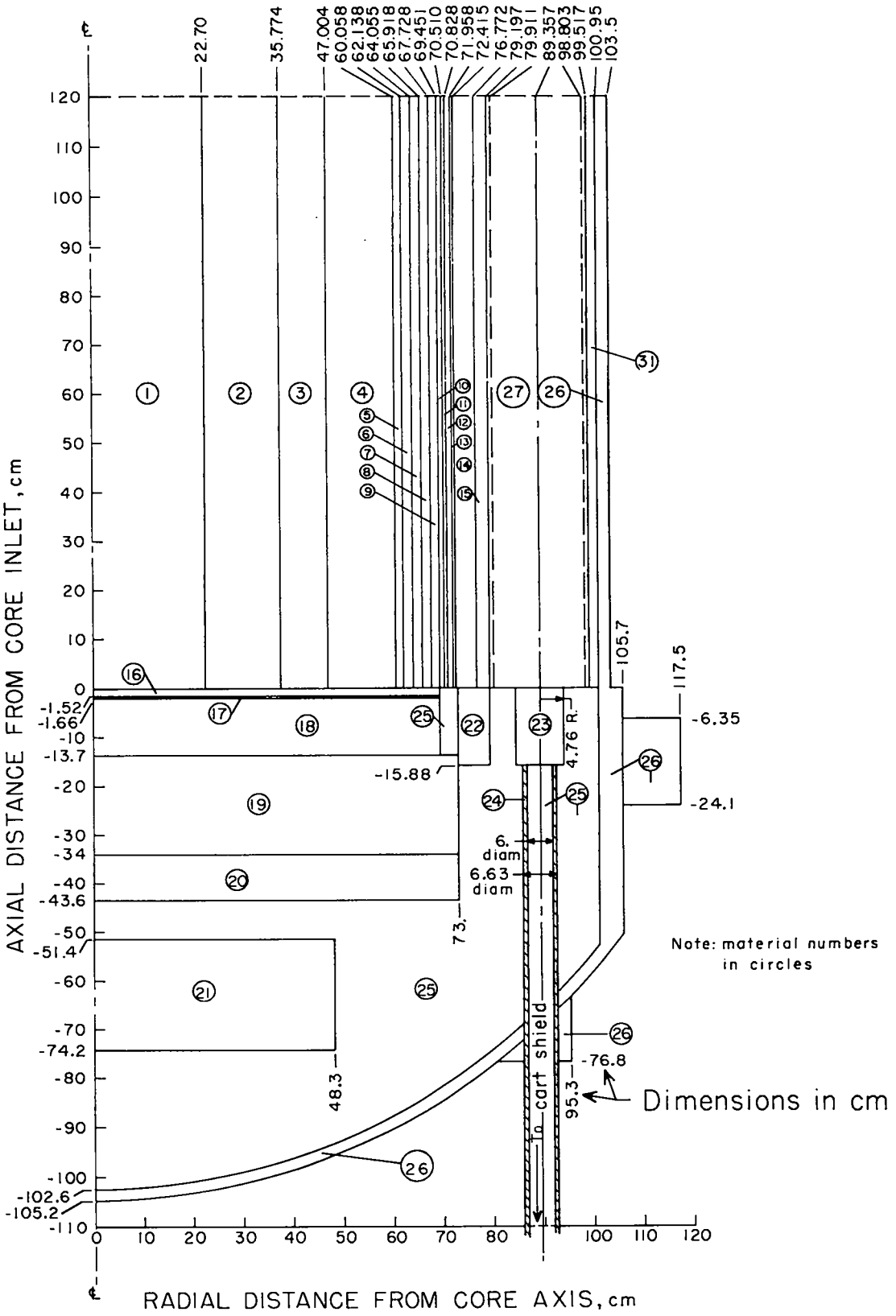

Fig. 13. Final calculational model, reactor fore end.

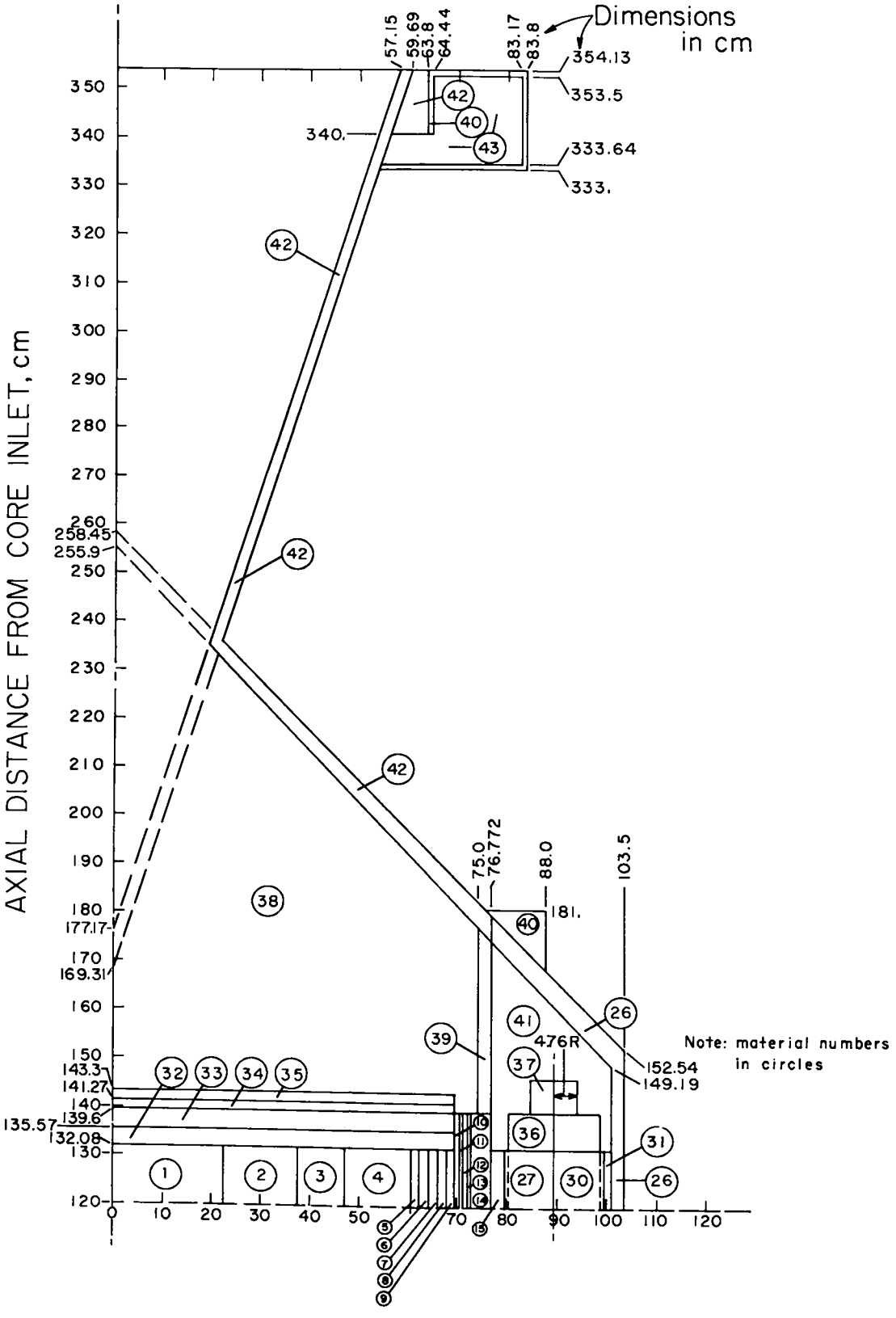

Fig. 14. Final calculational model, reactor aft end.

TABLE II

MATERIAL COMPOSITIONS FOR FINAL PHOEBUS 2A MODEL

Material Number	Atom Densities, atoms/cm^3 x 10^{-24}													
	^{235}U	^{238}U	C	Nb	Fe	Ni	Cr	Al	B	Ti	W	Be	H	O
1	0.000231	0.0000174	0.06108	0.001125	0.000058	0.000584	0.000152	--	--	--	--	--	--	--
2	0.000275	0.0000207	0.06087	0.001136	"	"	"	--	--	--	--	--	--	--
3	0.000357	0.0000269	0.06055	0.001128	"	"	"	--	--	--	--	--	--	--
4	0.000435	0.0000328	0.0598	0.001179	"	"	"	--	--	--	--	--	--	--
5	0.000397	0.0000299	0.06019	0.001164	"	"	"	--	--	--	--	--	--	--
6	0.000335	0.0000252	0.06079	0.001117	0.000061	0.000613	0.000159	--	--	--	--	--	--	--
7	0.000266	0.0000201	0.06103	0.001134	"	"	"	--	--	--	--	--	--	--
8	0.000197	0.0000148	0.06128	0.00114	"	"	"	--	--	--	--	--	--	--
9	0.0000883	0.00000664	0.06337	0.001223	0.000114	0.001152	0.000299	--	--	--	--	--	--	--
10	--	--	0.08948	0.0000324	--	--	--	--	--	--	--	--	--	--
11	--	--	0.1038	--	0.0028	0.00145	--	--	--	--	--	--	--	--
12	--	--	0.07958	--	0.000796	0.000684	0.000038	--	--	--	--	--	--	--
13	--	--	0.03813	--	--	--	--	--	--	--	--	--	--	--
14	--	--	0.00515	--	--	--	--	0.0536	--	--	--	--	--	--
15	--	--	--	--	--	--	--	--	--	--	--	--	--	--
16	--	--	0.0106	--	0.00335	0.000577	0.00015	0.00411	--	--	--	--	--	--
17	--	--	0.0135	--	0.0336	0.000577	0.00015	--	0.0115	--	--	--	--	--
18	--	--	0.00053	--	0.00144	0.00197	0.00105	0.000656	--	--	--	--	--	--
19	--	--	--	--	0.00035	0.00043	0.00022	0.04	--	--	--	--	--	--
20	--	--	--	--	0.00786	0.00125	0.0023	--	--	--	--	--	--	--
21	--	--	--	--	--	--	--	0.00199	--	--	--	--	--	--
22	--	--	--	--	--	--	--	0.068	--	--	--	--	--	--
23	--	--	--	--	0.0227	0.00359	0.00663	0.0063	--	0.0217	--	--	--	--
24	--	--	--	--	0.0286	0.0045	0.0084	--	--	--	--	--	--	--
25	--	--	--	--	--	--	--	--	--	--	--	--	--	--
26	--	--	--	--	--	--	--	0.0603	--	--	--	--	--	--
27	--	--	--	--	--	--	--	--	--	--	--	0.1073	--	--
28	--	--	--	--	--	--	--	0.0062	--	--	--	--	--	--
29	--	--	--	--	--	--	--	--	0.0427	--	--	--	--	--
30	--	--	--	--	--	--	--	0.0098	--	--	--	--	--	--
31	--	--	--	--	--	--	--	0.0404	--	--	--	--	--	--
32	--	--	0.06063	0.00213	0.000057	0.000577	0.00015	--	--	--	0.000174	--	--	--
33	--	--	0.0596	0.00269	0.000057	0.000577	0.00015	--	--	--	0.000174	--	--	--
34	--	--	0.0169	--	0.000057	0.000577	0.00015	--	--	--	0.000174	--	--	--
35	--	--	--	0.0022	0.00077	0.00318	0.00108	--	--	--	0.00603	--	--	--
36	--	--	--	--	0.00648	0.00104	0.00188	0.0436	--	0.00647	--	--	--	--
37	--	--	--	--	0.00305	0.00135	0.00246	--	--	0.0127	--	--	--	--
38	--	--	--	--	--	--	--	--	--	--	--	--	--	--
39	--	--	--	0.00339	0.0118	0.0279	0.0152	--	--	--	--	--	--	--
40	--	--	--	0.0045	0.0173	0.0373	0.0206	--	--	--	--	--	--	--
41	--	--	--	--	--	--	--	--	--	--	--	--	--	--
42	--	--	--	0.0023	0.009	0.0194	0.007	--	--	--	--	--	--	--
43	--	--	--	--	--	--	--	--	--	--	--	--	--	--
44	--	--	--	--	--	--	--	--	0.00112	--	--	--	0.0641	0.0341
45	--	--	--	--	0.0029	0.0081	0.0033	--	--	--	--	--	--	--

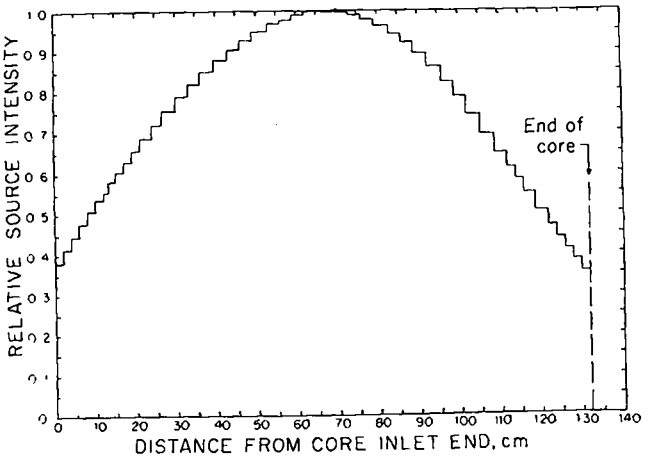

Fig. 15. Assumed axial distribution of neutron source.

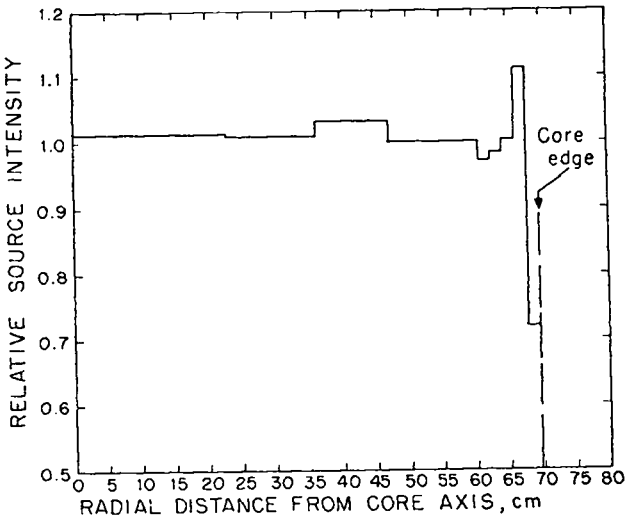

Fig. 16. Assumed radial distribution of neutron source.

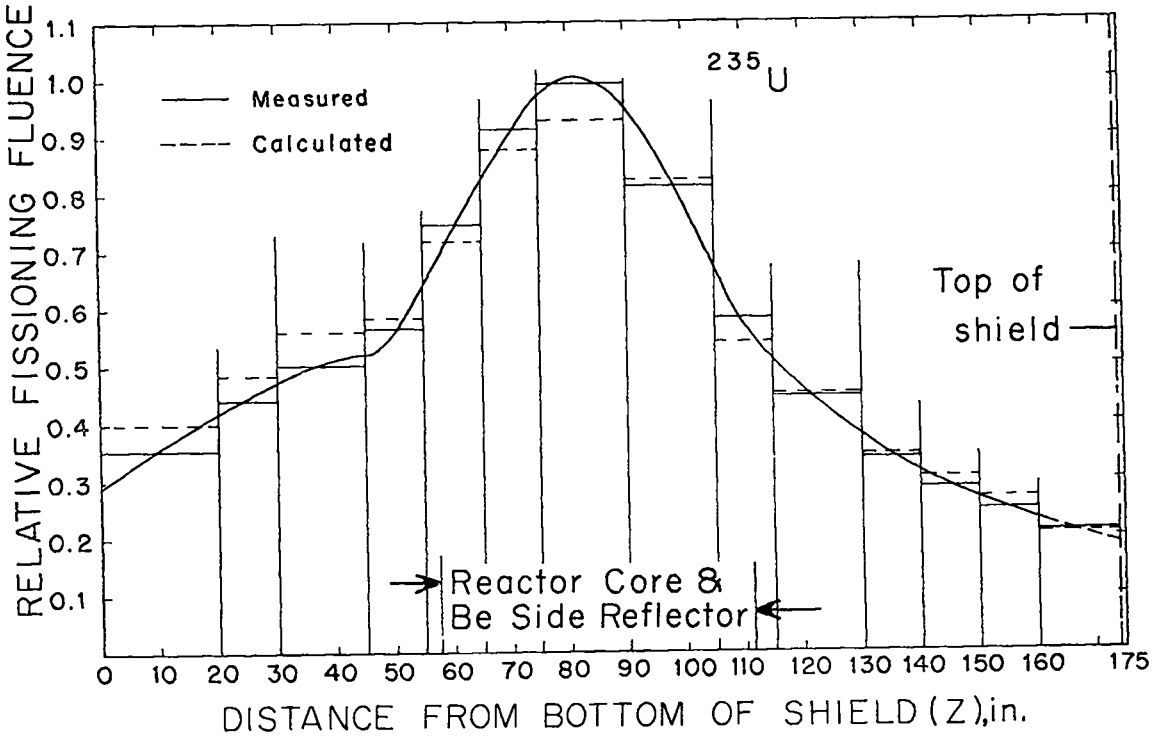

Fig. 17. Comparison of final calculations with experiment, ^{235}U axial distribution at shield inner surface.

The comparison is within the estimated uncertainty for most intervals, and is poor only for the extreme ends of the shield. Because the calculations included no air or other backscattering media above the shield, this result is to be expected at the shield upper end. The disagreement at the lower end of the shield, however, is not understood.

A more quantitative measure of the improvement in the final calculated axial distributions, as compared to the earlier values, is seen in Table III. A fundamental, and quite general improvement is evident in the final comparisons.

Calculated and measured radial fluence distributions opposite the core center, for ^{235}U and ^{238}U, are compared in Figs. 19 and 20. (Calculated data beyond ~ 15 in. into the shield were not statistically meaningful.) Again, agreement is excellent, being within one standard deviation except for the ^{235}U in the second and third aluminum layers. (For ^{235}U in these neutronically thin layers, the sta-

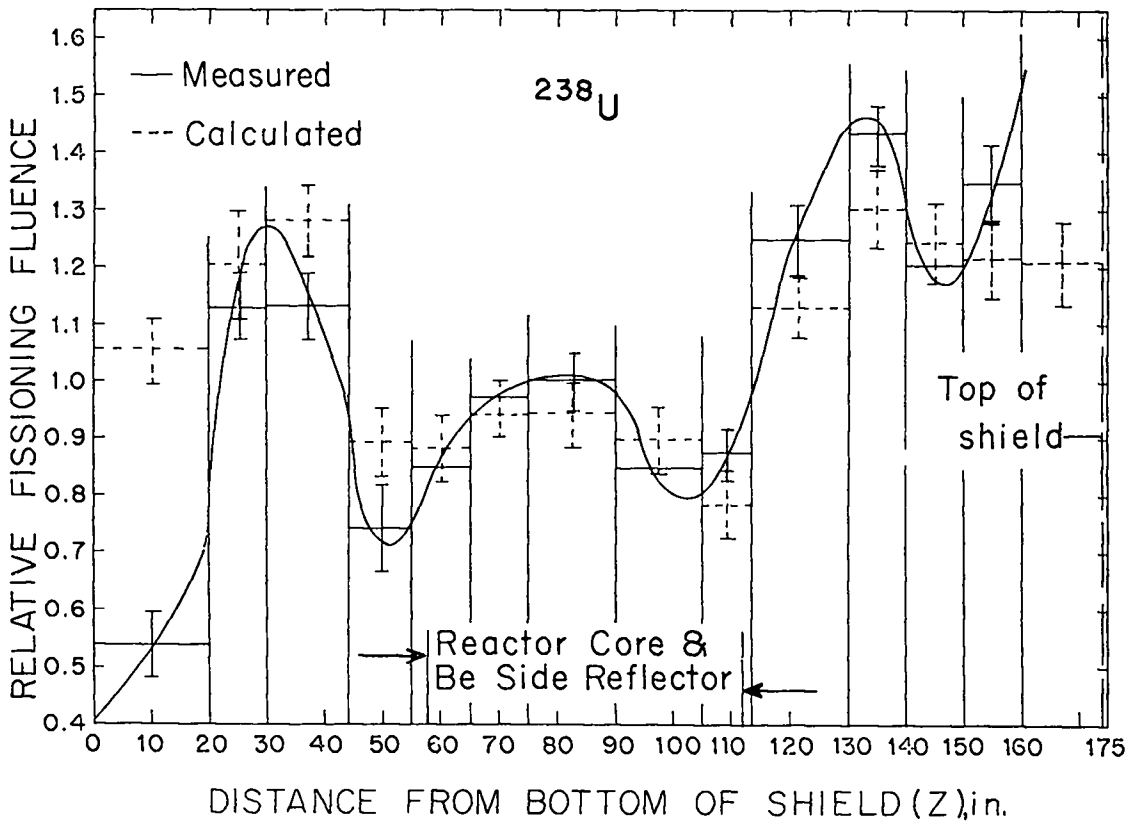

Fig. 18. Comparison of final calculations with experiment, ^{238}U axial distribution at shield inner surface.

TABLE III

RATIOS, MONTE CARLO-TO-MEASURED, FOR AXIAL FISSIONING FLUENCE DISTRIBUTIONS ALONG THE SHIELD INNER SURFACE. (DATA INTEGRATED OVER THE INDICATED ΔZ INTERVALS).

Z=Distance from Bottom of Shield		^{235}U (Overall Uncertainty ± 5 to 10%)		^{238}U (Overall Uncertainty ± 10 to 20%)	
Z, in.	ΔZ, in.	Initial Calculations	Final Calculations	Initial Calculations	Final Calculations
0 to 20	20	1.34	1.13	(1.40)	(1.96)
20 to 30	10	1.11	1.09	0.70	1.06
30 to 45	15	0.92	1.11	0.57	1.15
45 to 55	10	0.99	1.03	0.92	1.20
55 to 65	10	0.92	0.96	0.53	1.04
65 to 75	10	0.96	0.96	0.58	0.97
75 to 90	15	1.00	0.94	0.58	0.94
90 to 105	15	0.87	1.01	0.44	1.06
105 to 118	13	0.79	0.93	0.55	0.90
118 to 130	12	0.98	1.00	0.83	0.91
130 to 140	10	1.29	1.01	0.98	0.91
140 to 150	10	1.28	1.06	1.32	1.03
150 to 160	10	1.25	1.09	0.98	0.95
160 to 174	14	1.23	0.99	-	-

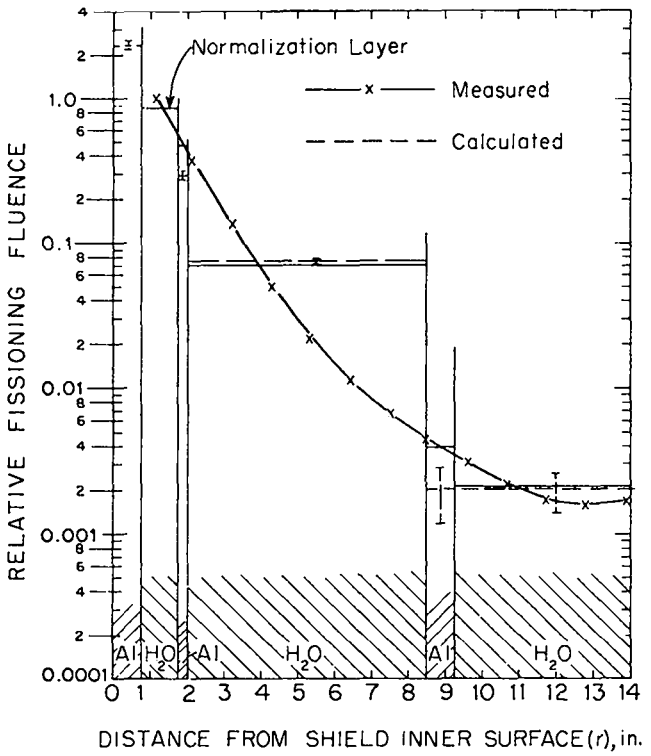

Fig. 19. Comparison of final calculations with experiment, ^{235}U radial distribution opposite core center.

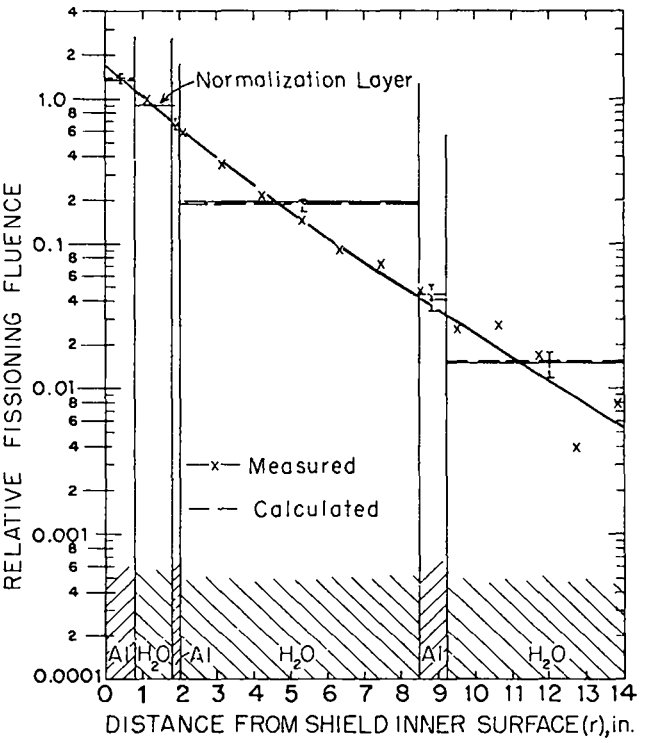

Fig. 20. Comparison of final calculations with experiment, ^{238}U radial distribution opposite core center.

tistical accuracy of the calculated relative error estimates is probably poor. Thus, the indicated error bars may be too small. This is much less likely in the borated-water regions and for all ^{238}U calculations.)

Table IV gives the final absolute comparisons between the measured and calculated core center-to-shield surface ratios. The ^{235}U comparison is good, whereas that for the ^{238}U is only fair. However, as mentioned earlier, the ^{238}U core-center data are suspect. A final summary of comparisons between calculated and measured results is given in Table V.

ACKNOWLEDGMENTS

Special thanks are due to the following LASL personnel for their contributions to this study. Counting techniques and equipment were primarily due to H. H. Helmick, including not only consultation and recommendations but also setup, calibration, and trouble-shooting of the counting equipment. L. W. McDonough provided support throughout this work, in hardware design for wire irradiations, in placement and recovery operations in Nevada, and in numerous other ways during the irradiations. Monte Carlo techniques and code developments were due to E. D. Cashwell and his associates, including J. R. Neergaard who did the coding for the IBM-7094 computer and G. D. Turner who was responsible for the CDC-6600 coding.

REFERENCES

1. C. W. Watson, "Measurement of ^{235}U and ^{238}U Fissioning Fluence Distributions in the Phoebus 2A Shield," Trans. Am. Nucl. Soc., 12, 382 (1969).
2. C. W. Watson, "Calculated Neutron Environment for Phoebus 2A," Trans. Am. Nucl. Soc., 13, 11 (1970).

TABLE IV

RATIOS OF FISSIONING FLUENCES, CORE CENTER-TO-SHIELD INNER SURFACE OPPOSITE THE CORE CENTER

	^{235}U	^{238}U
Measured	5.2	480
Calculated	4.8	300
Calculated ÷ measured	0.92	0.63

TABLE V

FINAL SUMMARY OF COMPARISONS BETWEEN CALCULATION AND EXPERIMENT

Quantity	Error in Final Calculations, % (Comparison with Experiment)
^{235}U, relative fissioning fluence distribution, axially at shield inner surface	< 10
^{238}U, relative fissioning fluence distribution, axially at shield inner surface	< 10 to 20 (except at extreme ends of shield)
^{235}U, relative fluence, radial distribution opposite core center	< 10 (except in thin Al regions)
^{238}U, relative fluence, radial distribution opposite core center	< 5
^{235}U, core center-to-shield surface ratio	< 10
^{238}U, core center-to-shield surface ratio	< 70[a]
^{235}U, implied absolute agreement in shield	10 to 30
^{238}U, implied absolute agreement in shield	20 to 100[a]

[a]The measured core center data here are in doubt.

3. C. W. Watson, "Fissioning Neutron Fluence Distributions in the Phoebus 1B Facility Shield," LASL Report LA-4166 (1969).
4. W. U. Geer, P. G. Koontz, J. D. Orndoff, H. C. Paxton, "Safety Analysis for the Los Alamos Critical-Assembly Facility," LASL Report LA-4273. (1969).
5. E. D. Cashwell, Unpublished.
6. R. R. Johnston, "A General Monte Carlo Neutronics Code," LASL Report LAMS-2856. (1963).
7. W. W. Clendenin, "The Monatomic Gas Model for Thermal Neutron Distributions in a Physical Moderator," Nucl. Energy, Part A; Reactor Science, 13, 25 (1960)
8. E. D. Cashwell, LASL, private communication.

APPENDIX A

EVALUATION OF ^{238}U WIRE DEPLETION FOR THE PHOEBUS 2A MEASUREMENTS

Satisfactory ^{235}U depletion of the ^{238}U wire used in the Phoebus 2A shield measurements was of considerable concern. Several direct mass-spectrographic analyses of the wire were inconclusive, possibly because of contamination from unknown sources during preparation of the samples. Although most (but not all) of these analyses indicated adequate depletion, the depletions were generally less than the expected 2 ppm ^{235}U. Other determinations were, therefore, considered necessary.

Another check was made by irradiating ^{235}U and ^{238}U wires radially across the outlet end of the PARKA critical assembly, where the neutron spectrum varied from relatively hard at the core center (^{235}U:^{238}U ratio, < 100) to quite soft across the beryllium reflector (^{235}U:^{238}U ratio, > 1000). The fissioning-fluence distributions in the two wires, were expected, therefore, to be distinctively different. The results, plotted in Fig. A-1, show that the distributions were qualitatively as expected. There was no indication that the ^{238}U distribution was contaminated by ^{235}U fissions, and the ^{238}U data exhibited a rather classical cosine-like shape, to be expected for the fast-flux distribution.

In still another check, in the Pewee 1 Zepo assembly (a zero-power mockup of the first of the LASL Pewee series of Rover reactors), ^{238}U wires with lower, but known, depletions (~ 2000 to 4000:1) were irradiated in various locations simultaneously with Phoebus 2A ^{238}U wires. Counting rates were then compared to display differences due to differences in ^{235}U content. In principle, the ^{235}U content of the Phoebus 2A wires could be determined from these data and from the known depletions of the other wires; however, at the 2-ppm level, small uncertainties in the data and in the depletions of the "known" ^{238}U wires led to large errors in the estimation of the unknown depletion. Again, distinctive differences were observed which indicated that the depletion of the Phoebus 2A wire was considerably larger than that of the other samples.

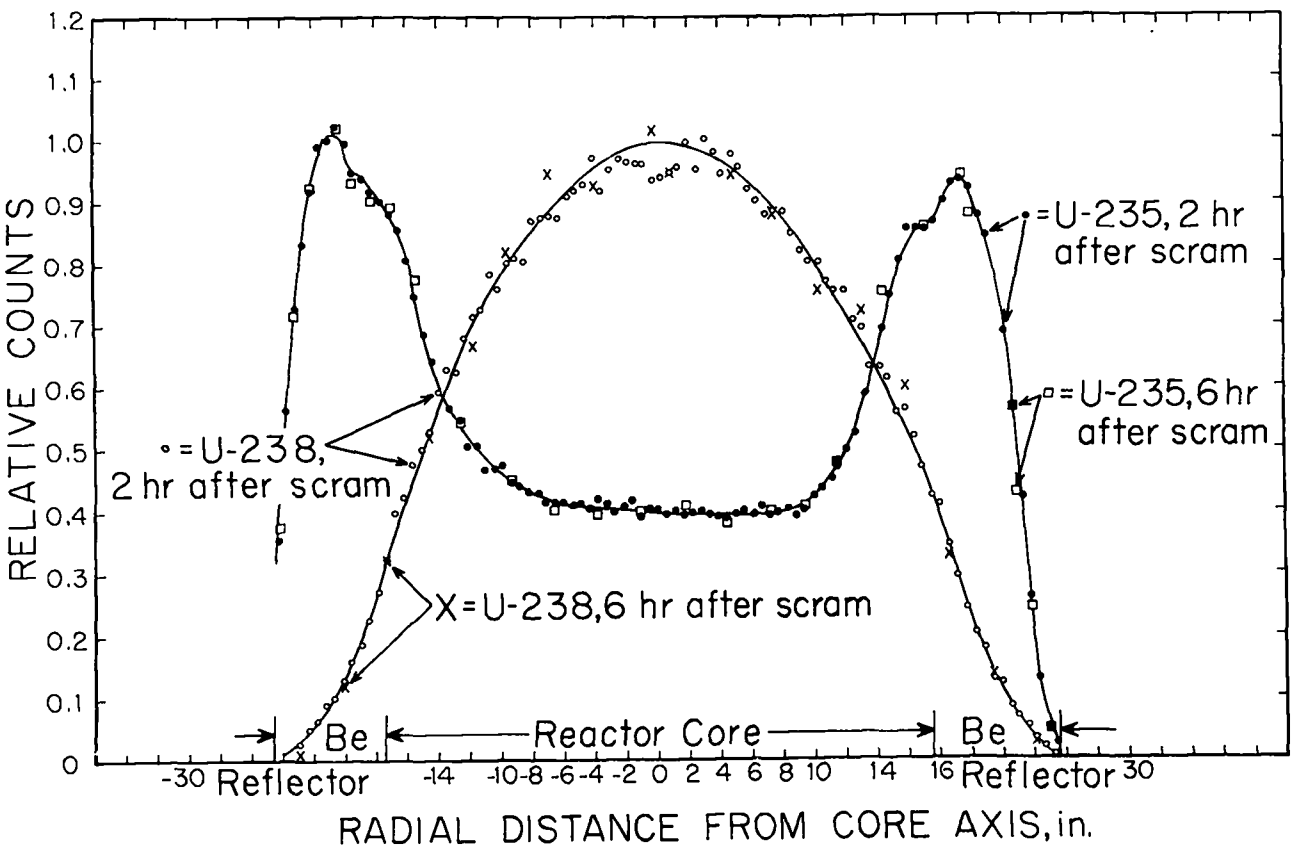

Fig. A-1. ^{235}U and ^{238}U traverses across outlet end of PARKA.

Also, a series of ^{235}U and ^{238}U axial fissioning-fluence distributions was measured in the Phoebus-1B shield during the NRX-A6 tests at the Nevada Test Site (Nov., 1967). The NRX-A6 (an Aerojet-Westinghouse NERVA test reactor) was neutronically similar to the Phoebus 1B reactor and used the same shield. Thus, considerable neutronics data directly applicable to these tests, including data for the shield,were available at IASL. It was known, for example, that the ^{235}U and ^{238}U distributions in the shield should be similar but distinguishable. Directly applicable Monte Carlo results were also available. The NRX-A6 data for ^{235}U compared well with both the calculated and the measured Phoebus 1B results. The ^{238}U transverses for NRX-A6, using the Phoebus 2A wire, were in fair agreement with the Phoebus 1B calculations, and were characteristically different from the NRX-A6 ^{235}U transverses.

Finally, IASL Group J-11 carefully analysed for ^{235}U in a Phoebus 2A ^{238}U wire by fission-fragment counting. In this technique, an accurately weighed sample is deposited as a very thin foil and irradiated in a known, very thermal, neutron-flux field (the reflector of the IASL Water-Boiler reactor). During irradiation, the escaping fission fragments are counted, and, since they can (almost) all be attributed to ^{235}U, the absolute ^{235}U content can be determined. This analysis estimated the ^{235}U content in the wire to be $\leq$ 2 ppm, which is the approximate lower limit of usefulness for the technique.

APPENDIX B

FISSIONING FLUENCE DISTRIBUTIONS ALONG PHOEBUS 2A CART-SHIELD AXIS

Fissioning-fluence traverses along the axis of the Phoebus 2A reactor cart shield are shown in Fig. B-1. They are very similar to those measured radially in the facility shield, at least at distances greater than ~ 6 in. into the shield. This is to be expected, because neutron transport in both shields is determined primarily by the borated water, and the asymptotic relaxation length in all cases is the relaxation length characteristic of Phoebus 2A fast leakage neutrons in the water.

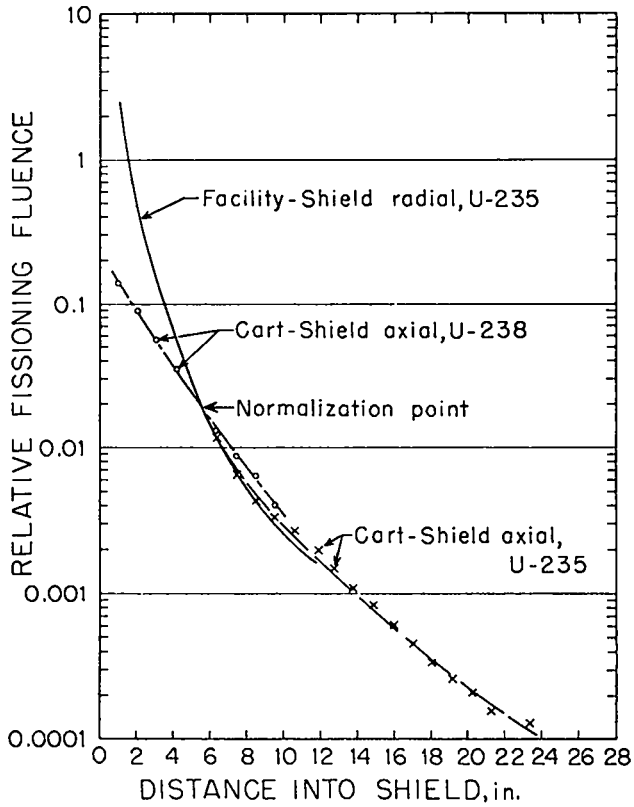

Fig. B-1. ^{235}U and ^{238}U fissioning fluence distributions along axis of Phoebus 2A cart shield.

APPENDIX C

ALUMINUM ABSORPTION DISTRIBUTIONS IN PHOEBUS 2A SHIELD

Distributions of ^{65}Zn activity in aluminum samples taken ~ 500 days after the Phoebus 2A tests are shown in Fig. C-1 for the top surface of the cart shield, in Fig. C-2 for a traverse across the top of the facility shield, and in Fig. C-3 for an axial traverse at the inner surface of the facility shield. The distribution in Fig. C-2 is compared with the previously-described ^{235}U traverse, and a calculated absorption-rate distribution, from Appendix D, is compared with the measured distribution of Fig. C-3. The differences in Figs. C-2 and C-3 probably result from the fact that the measured absorption curves give neutron absorptions from the total Phoebus 2A test series, most of which included hydrogen in the reactor (particularly at the inlet end). On the other hand, the ^{235}U curve in Fig. C-2 and the calculated distribution in Fig. C-3 correspond to runs in which the reactor did not contain hydrogen.

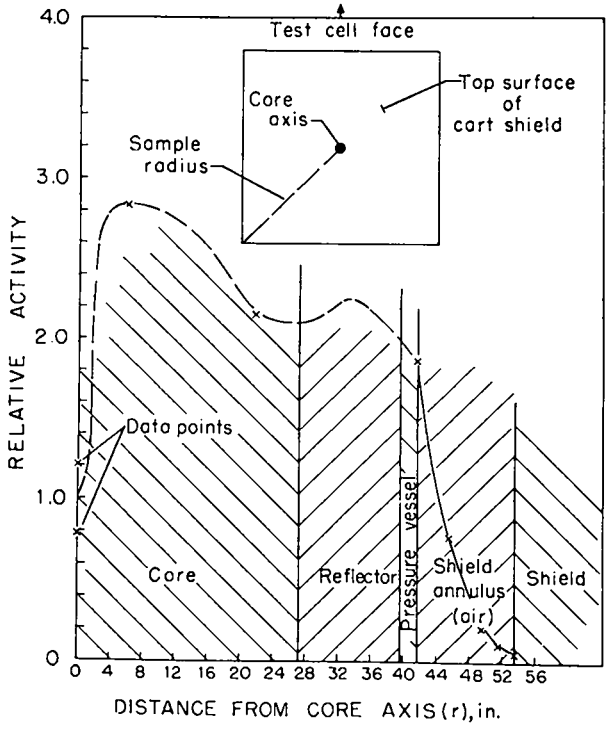

Fig. C-1. Measured distribution of residual γ-activity across top of cart shield.

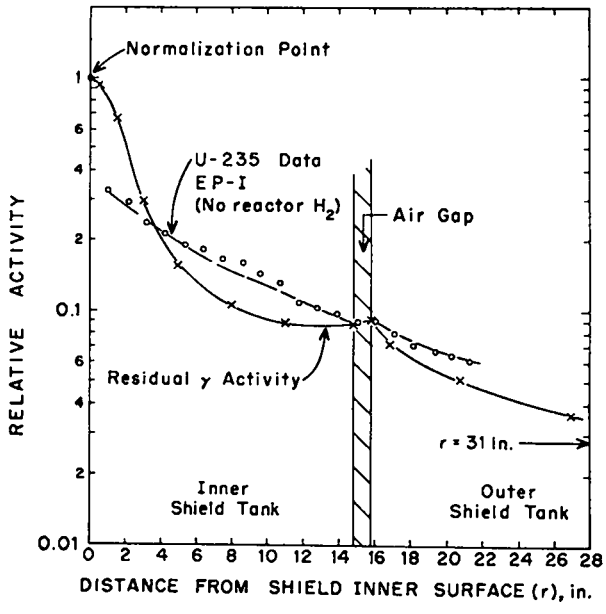

Fig. C-2. Measured distribution of residual γ-activity across top of facility shield, comparison with measured ^{235}U fissioning fluence distribution.

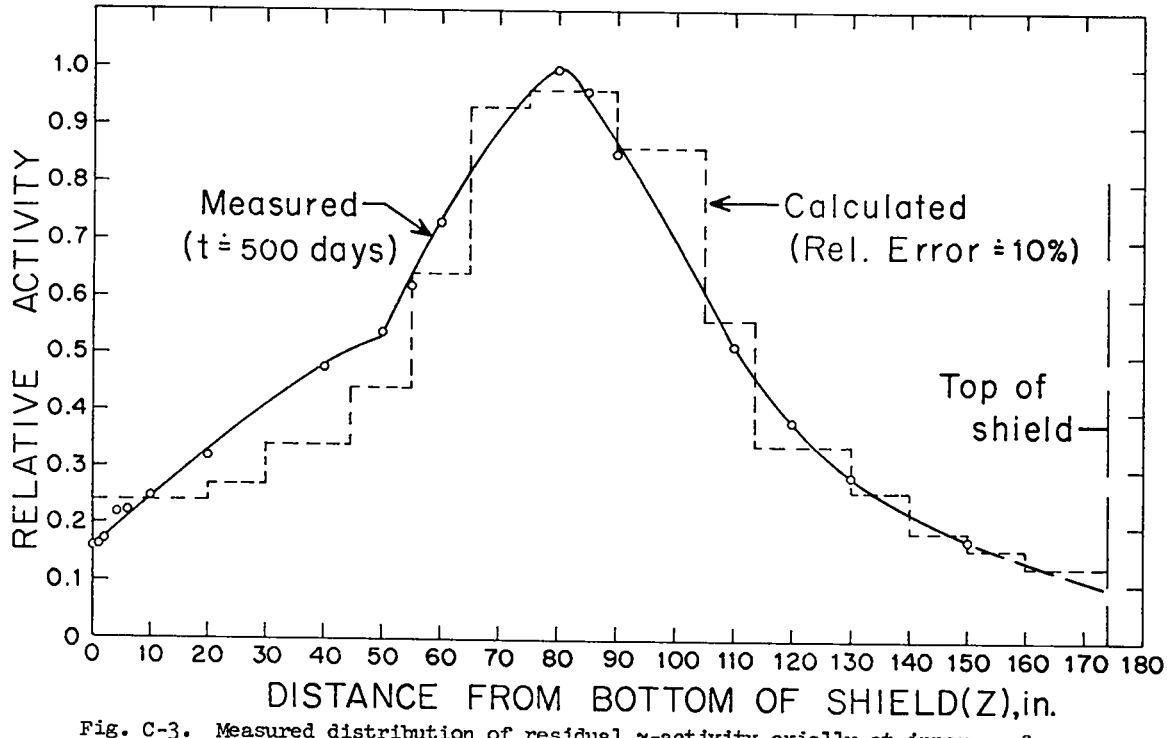

Fig. C-3. Measured distribution of residual γ-activity axially at inner surface of facility shield, comparison with calculated absorption distribution.

APPENDIX D

CALCULATED ABSORPTION AND FISSION RATES

Figures D-1, D-2, D-3, and D-4 (in conjunction with Figs. 9, 12, 13, and 14 in the body of the report) identify tally cells for the final calculations. The cell numbers correspond to those in Tables D-I, D-II, and D-III, where cell volumes, calculated fission rates, and calculated total neutron-absorption rates are given for two different control-drum positions. All tally cells are cylindrically symmetric except some control-drum cells and those cells through which the control drums and actuators pass, e.g., Cells 104 to 112 and Cells 78 to 80. All 18 control drums are lumped together for the tallies. For example, Cell 161 represents 18 identical physical regions (beryllium drums), and the absorption rate given in Table D-I for Cell 161 is the total for all 18 regions. The same is true for the other control-drum regions shown in Fig. D-4. In Fig. D-4, twelve different control-vane cells are shown, each corresponding to 30° of the total vane rotation; the calculated control-drum position was fixed, in 30° increments, by loading these regions with boron or unloading them, e.g., boron in Cells 164, 165, 166, and 167 corresponds to a control-drum position of 90°.

The values in Tables D-I through D-III correspond to ~ 5000 MW total fission power using the normalization factor

$$\beta = 4.034 \times 10^{20} \text{ neutrons produced/5000 MW fission power.}^{*}$$

---

*Note again, that these calculations correspond to EP's -1 and -2 (wire irradiations), and include no hydrogen in the reactor.

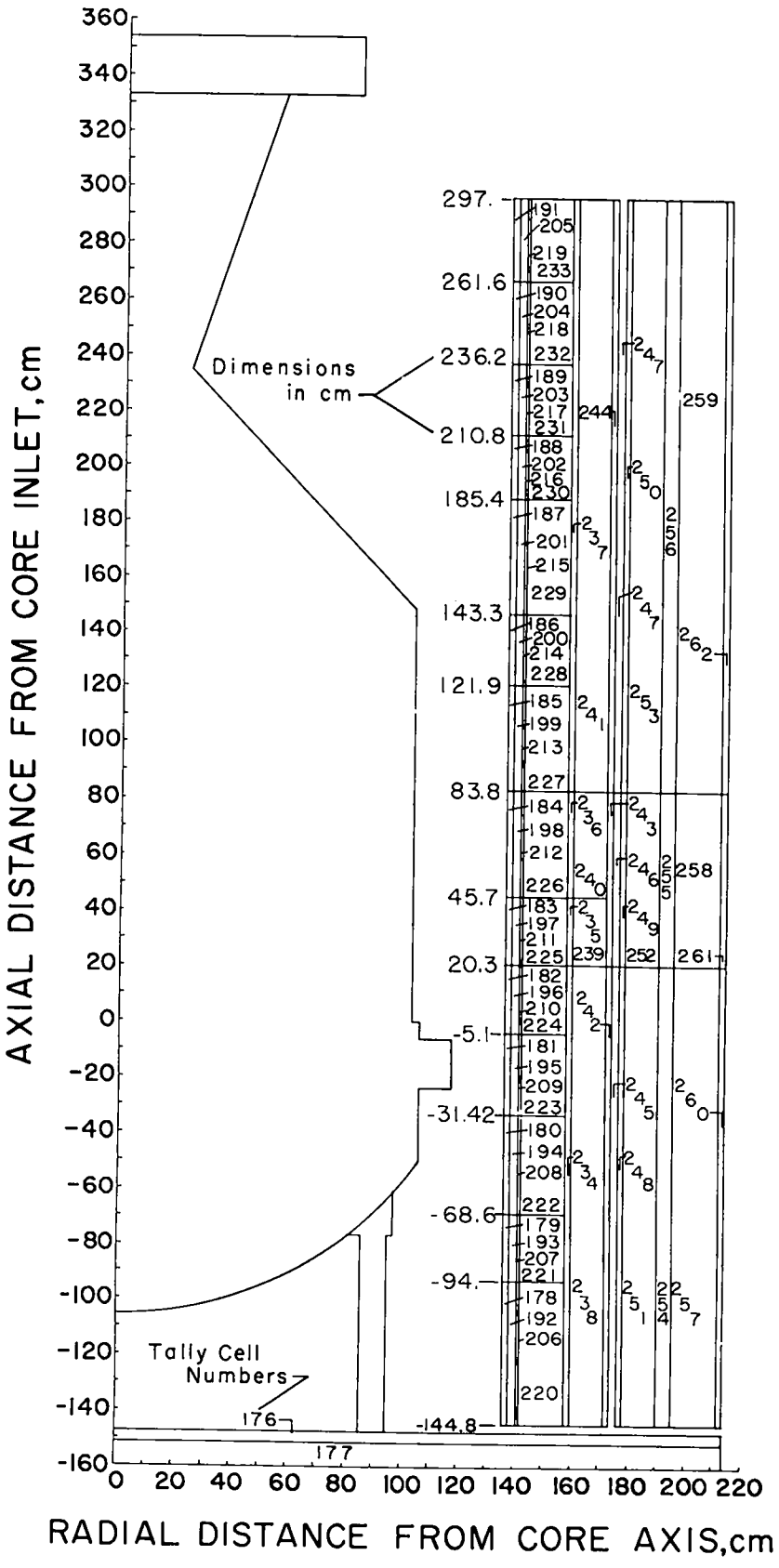

Fig. D-1. Final calculational model, tally cells in cart and facility shields.

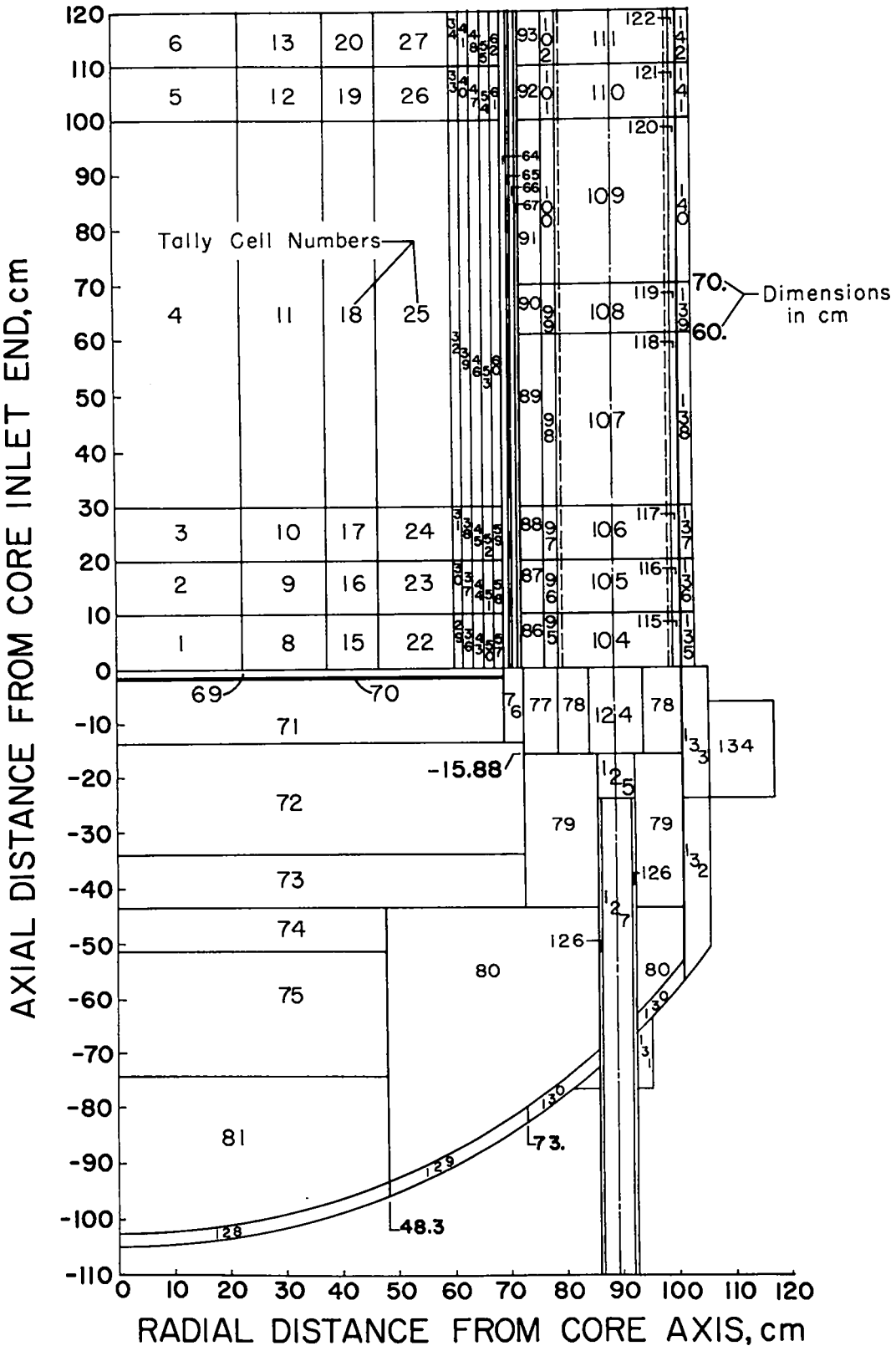

Fig. D-2. Final calculational model, tally cells in reactor fore end.

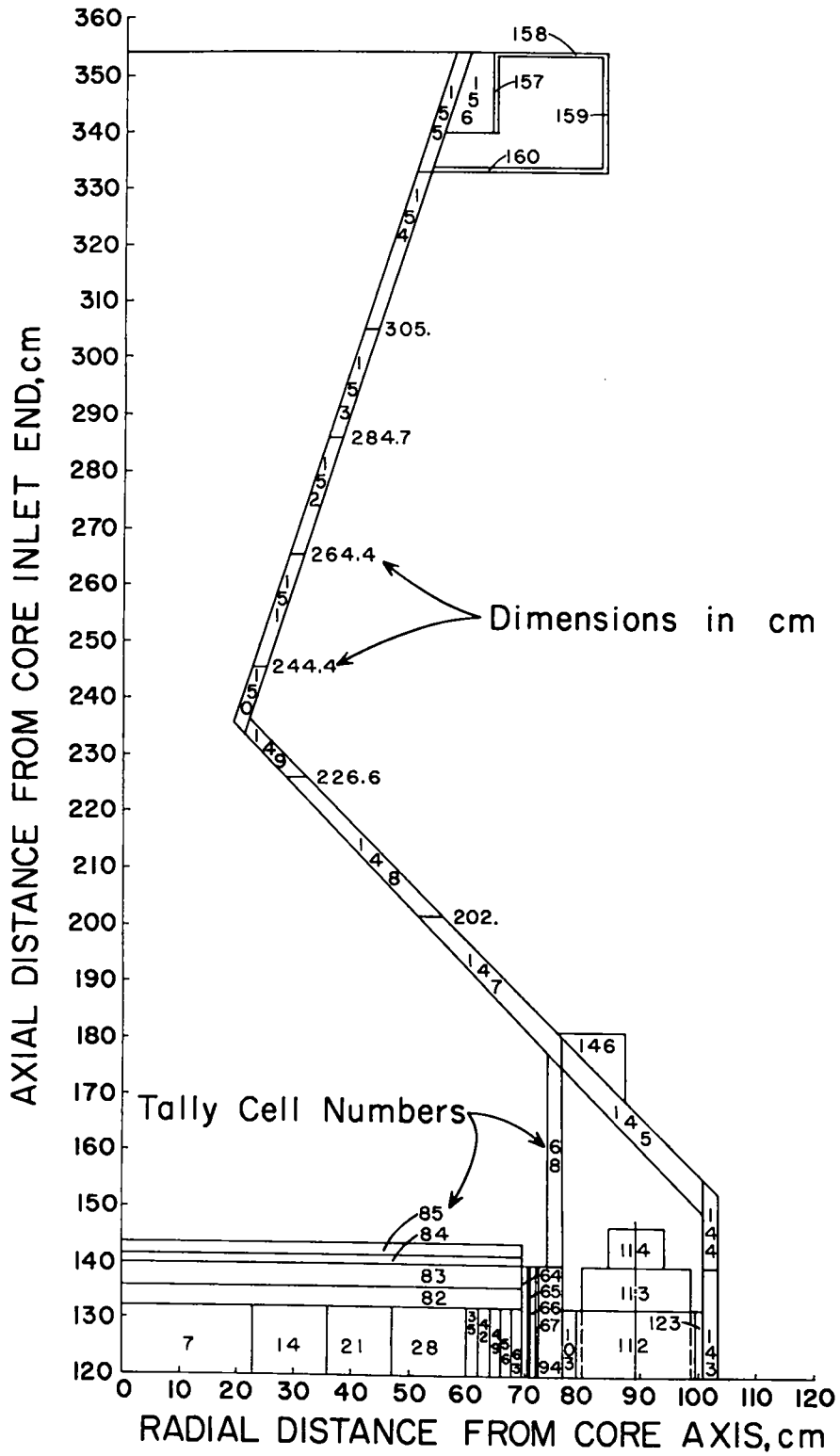

Fig. D-3. Final calculational model, tally cells in reactor aft end.

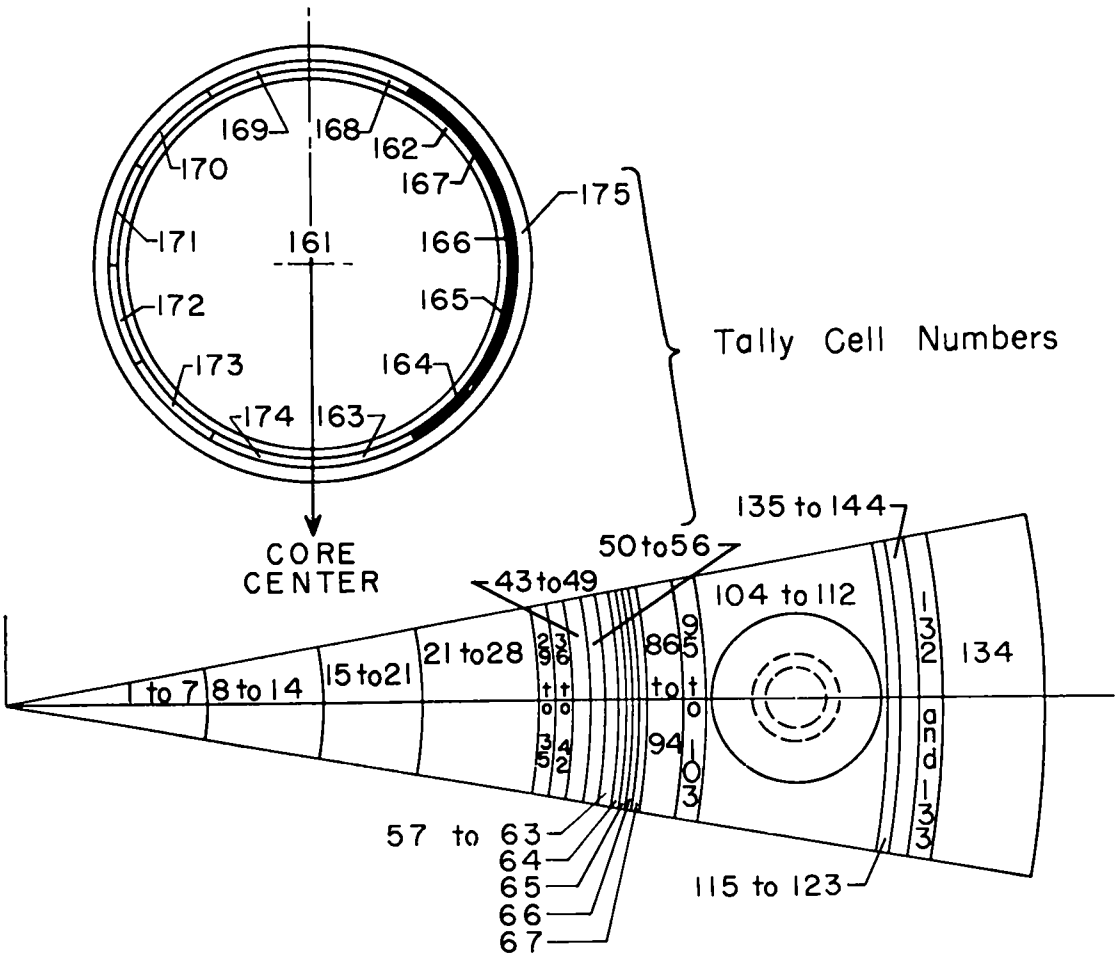

Fig. D-4. Final calculational model, tally cells in control drums.

TABLE D-I

CALCULATED NEUTRON ABSORPTION RATES
(EXCLUDING FISSION) FOR 5000-MW PHOEBUS 2A

Cell No.	Cell Volume, cm^3	Control Drum at 90°		Control Drum at 120°		Cell No.	Cell Volume, cm^3	Control Drum at 90°		Control Drum at 120°	
		10^{-17} x Absorptions/sec	Rel. Error, %	10^{-17} x Absorptions/sec	Rel. Error, %			10^{-17} x Absorptions/sec	Rel. Error, %	10^{-17} x Absorptions/sec	Rel. Error, %
1	1.619 + 4 [a]	4.82	6	5.22	5	67	2.894 + 4	0.061	6	0.088	18
2	"	8.30	5	8.83	5	68	3.048 + 4	4.63	5	5.46	5
3	"	10.8	6	10.5	6	69	2.303 + 4	0.706	6	0.678	5
4	1.133 + 5	103	3	99.4	3	70	2.121 + 3	10.3	5	11.6	6
5	1.619 + 4	11.0	6	11.3	6	71	1.824 + 5	3.79	4	3.88	4
6	"	9.01	5	8.71	6	72	3.399 + 5	6.59	4	6.63	4
7	1.956 + 4	7.37	5	6.89	5	73	1.607 + 5	4.03	4	4.17	5
8	2.402 + 4	7.56	4	7.32	4	74	5.717 + 4	--	-	--	-
9	"	11.5	4	11.7	5	75	1.671 + 5	0.054	16	0.067	18
10	"	15.6	5	14.9	5	76	2.176 + 4	--	-	--	-
11	1.681 + 5	138	3	135	2	77	4.705 + 4	2.02	5	2.28	6
12	2.402 + 4	15.4	5	15.5	5	78	1.752 + 5	--	-	--	-
13	"	11.5	4	12.1	4	79	4.062 + 5	--	-	--	-
14	2.901 + 4	10.3	4	10.3	4	80	7.277 + 5	--	-	--	-
15	2.920 + 4	7.96	5	8.51	4	81	1.735 + 5	--	-	--	-
16	"	13.4	4	14.1	4	82	5.288 + 4	19.5	4	20.8	4
17	"	18.8	6	16.1	5	83	6.107 + 4	13.7	4	14.7	4
18	2.044 + 5	179	3	162	3	84	2.531 + 4	1.48	9	1.57	11
19	2.920 + 4	17.4	6	19.4	5	85	3.076 + 4	17.5	4	18.5	4
20	"	14.6	6	14.4	5	86	2.042 + 4	1.89	5	2.37	6
21	3.528 + 4	11.4	4	12.1	5	87	"	3.53	5	4.11	5
22	4.391 + 4	12.1	5	11.3	5	88	"	4.59	5	5.31	4
23	"	18.3	5	19.2	5	89	6.126 + 4	17.8	3	22.4	4
24	"	22.9	5	23.6	5	90	2.042 + 4	6.40	5	8.10	4
25	3.073 + 5	225	3	227	3	91	6.126 + 4	18.3	4	22.4	3
26	4.391 + 4	26.4	6	27.8	6	92	2.042 + 4	4.93	5	5.72	4
27	"	19.0	5	22.1	5	93	"	3.86	6	4.60	5
28	5.304 + 4	14.8	4	16.1	4	94	4.002 + 4	3.09	5	4.18	5
29	7985	2.05	9	1.80	10	95	1.188 + 4	--	-	--	-
30	"	3.29	8	3.34	8	96	"	--	-	--	-
31	"	3.67	7	4.08	7	97	"	--	-	--	-
32	5.589 + 4	36.2	3	38.5	4	98	3.565 + 4	--	-	--	-
33	7985	3.66	6	4.30	7	99	1.188 + 4	--	-	--	-
34	7985	3.02	7	3.38	9	100	3.565 + 4	--	-	--	-
35	9646	2.47	8	2.91	8	101	1.188 + 4	--	-	--	-
36	7600	1.74	9	1.56	9	102	"	--	-	--	-
37	"	2.61	8	2.33	7	103	1.435 + 4	--	-	--	-
38	"	3.42	7	3.39	6	104	6.363 + 4	0.698	7	0.698	6
39	5.320 + 4	33.5	4	34.7	4	105	"	1.06	6	1.16	5
40	7600	3.22	7	3.99	10	106	"	1.44	5	1.67	5
41	"	2.96	8	3.13	8	107	1.909 + 5	5.66	3	6.04	3
42	9181	2.53	8	2.92	8	108	6.363 + 4	2.04	5	2.41	4
43	7607	1.44	9	1.48	10	109	1.909 + 5	5.53	4	6.33	3
44	"	2.31	8	2.82	8	110	6.363 + 4	1.44	5	1.61	4
45	"	3.06	7	3.38	8	111	"	1.14	6	1.36	5
46	5.325 + 4	31.5	4	31.8	4	112	7.687 + 4	0.851	6	0.904	5
47	7607	3.02	9	3.38	7	113	3.794 + 4	4.39	7	4.52	6
48	"	2.59	8	2.73	7	114	8969	0.662	20	0.662	11
49	9189	1.61	8	2.18	8	115	9025	0.17	16	0.24	37
50	7599	1.36	9	1.63	10	116	"	0.29	18	0.20	15
51	"	2.13	8	2.17	8	117	"	0.24	13	0.24	15
52	"	3.45	7	3.51	8	118	2.707 + 4	1.2	9	0.912	8
53	5.320 + 4	28.0	3	29.3	3	119	9025	0.53	14	0.34	12
54	7599	3.45	8	3.85	9	120	2.707 + 4	1.1	8	1.11	9
55	"	2.53	10	2.92	9	121	9025	0.32	13	0.34	14
56	9180	1.89	11	1.94	8	122	"	0.22	16	0.28	14
57	7425	1.15	12	1.32	11	123	1.090 + 4	0.31	32	0.22	22
58	"	1.81	10	2.05	9	124	2.035 + 4	4.88	6	5.33	6
59	"	2.39	9	2.55	7	125	5108	0.24	19	0.35	19
60	5.198 + 4	22.9	3	25.9	3	126	1.386 + 4	0.900	6	1.13	7
61	7425	2.72	8	2.75	7	127	--	--	-	--	-
62	"	2.22	11	2.40	10	128	1.979 + 4	0.15	12	0.17	16
63	8970	1.42	9	1.81	10	129	2.801 + 4	0.27	9	0.26	9
64	6.500 + 4	0.58	14	0.52	7	130	5.394 + 4	0.56	7	0.61	6
65	1.971 + 4	3.71	4	4.68	4	131	4.880 + 4	0.47	8	0.43	7
66	7.076 + 4	5.70	4	6.94	4	132	9.069 + 4	1.07	6	1.19	6

[a] $1.619 + 4 = 1.619 \times 10^4$

TABLE D-I (continued)

Cell No.	Cell Volume, cm^3	Control Drum at 90° 10^{-17} x Absorptions/sec	Rel. Error, %	Control Drum at 120° 10^{-17} x Absorptions/sec	Rel. Error, %
133	7.432 + 4	1.27	7	1.23	6
134	1.469 + 5	1.93	7	1.74	6
135	1.638 + 4	0.37	13	0.32	11
136	"	0.61	18	0.54	10
137	1.638 + 4	0.690	11	0.625	11
138	4.914 + 4	2.39	6	2.33	7
139	1.638 + 4	1.02	9	0.924	11
140	4.914 + 4	2.40	6	2.18	6
141	1.638 + 4	0.706	10	0.524	11
142	"	0.545	11	0.456	10
143	3.210 + 4	0.597	11	0.577	12
144	2.331 + 4	0.347	12	0.38	14
145	7.517 + 4	0.904	6	1.17	8
146	4.091 + 4	3.81	6	4.06	6
147	4.605 + 4	3.67	5	4.41	5
148	2.437 + 4	0.722	7	0.887	9
149	4532	0.212	10	0.22	12
150	3267	0.135	17	0.18	36
151	8365	0.19	17	0.14	14
152	1.060 + 4	0.20	15	0.19	18
153	1.272 + 4	0.20	20	0.21	16
154	2.099 + 4	0.29	13	0.27	13
155	1.851 + 4	0.19	20	0.15	16
156	3.431 + 4	0.24	15	0.21	14
157	3643	0.049	27	0.06	21
158	5472	0.071	17	0.10	18
159	6983	0.128	19	0.16	18
160	8267	0.276	13	0.35	22
161	5.235 + 5	12.7	2	14.5	2
162	6.572 + 4	1.48	7	1.75	6
163	2849	0.799	8	1.12	6
164	2849	134	2	0.976	8
165	2849	99.6	3	139	2
166	2849	62.1	3	73.0	3
167	2849	43.1	4	37.5	4
168	2849	0.266	15	39.6	4
169	2849	0.304	13	0.444	14
170	2849	0.734	10	0.718	10
171	2849	1.02	8	1.16	8
172	2849	1.27	7	1.49	7
173	2849	1.18	7	1.43	7
174	2849	0.855	7	1.23	8
175	4.302 + 4	1.67	7	1.98	5
176	6.295 + 5	1.91	5	2.14	5
177	--	77.8	3	81.2	2
178	8.299 + 4	0.565	7	0.569	6
179	4.150 + 4	0.333	8	0.322	8
180	6.074 + 4	0.621	8	0.581	6
181	4.300 + 4	0.532	7	0.569	8
182	4.150 + 4	0.762	7	0.766	8
183	4.150 + 4	1.21	8	1.00	6
184	6.224 + 4	1.80	6	1.65	5
185	6.224 + 4	1.57	8	1.51	5
186	3.496 + 4	0.645	10	0.484	9
187	6.878 + 4	0.658	8	0.682	7
188	4.150 + 4	0.311	11	0.31	13
189	4.150 + 4	0.214	11	0.232	8
190	4.150 + 4	0.184	9	0.191	9
191	5.816 + 4	0.231	12	0.209	11
192	1.110 + 5	27.0	3	26.9	3
193	5.548 + 4	16.1	4	16.3	4
194	8.121 + 4	26.1	3	27.5	3
195	5.749 + 4	20.5	4	20.3	4
196	5.548 + 4	24.9	4	24.8	4
197	5.548 + 4	32.4	4	29.1	4
198	8.322 + 4	50.3	3	49.6	3
199	8.322 + 4	46.8	3	40.7	3
200	4.674 + 4	16.5	4	16.1	4
201	9.195 + 4	25.4	4	25.2	4
202	5.548 + 4	11.2	5	12.4	5
203	5.548 + 4	9.44	5	10.6	5
204	5.548 + 4	8.89	5	9.01	5
205	7.776 + 4	9.60	5	9.14	5
206	3.143 + 4	0.098	11	0.086	9
207	1.571 + 4	0.059	11	0.072	15
208	2.300 + 4	0.095	9	0.102	12
209	1.628 + 4	0.068	16	0.058	12
210	1.571 + 4	0.083	21	0.060	20
211	1.571 + 4	0.053	17	0.061	20
212	2.357 + 4	0.075	15	0.101	24
213	2.357 + 4	0.075	18	0.080	13
214	1.324 + 4	0.036	20	0.051	22
215	2.604 + 4	0.096	13	0.078	13
216	1.571 + 4	0.039	17	0.039	19
217	1.571 + 4	0.033	15	0.035	13
218	1.571 + 4	0.031	14	0.035	14
219	2.202 + 4	0.038	15	0.031	12
220	7.860 + 5	21.8	3	22.0	3
221	3.930 + 5	12.8	4	12.8	4
222	5.753 + 5	23.1	3	21.2	3
223	4.073 + 5	12.4	4	12.7	4
224	3.930 + 5	11.0	5	11.5	4
225	3.930 + 5	10.3	6	9.27	5
226	5.895 + 5	14.1	5	14.5	5
227	5.895 + 5	13.6	5	13.3	5
228	3.311 + 5	7.65	5	8.28	6
229	6.514 + 5	17.0	4	18.7	4
230	3.930 + 5	9.65	4	10.5	5
231	3.930 + 5	8.88	5	9.83	5
232	3.930 + 5	8.26	5	8.38	5
233	5.508 + 5	9.28	5	8.16	5
234	3.123 + 5	0.006	31	0.065	33
235	4.805 + 4	--	-	--	-
236	7.207 + 4	--	-	--	-
237	4.037 + 5	--	-	--	-
238	2.077 + 6	0.89	11	0.694	11
239	3.195 + 5	0.07	37	0.04	45
240	4.792 + 5	0.17	32	0.19	30
241	2.684 + 6	0.87	12	0.57	12
242	3.399 + 5	--	-	--	-
243	1.307 + 5	--	-	--	-
244	4.393 + 5	--	-	--	-
245	--	--	-	--	-
246	--	--	-	--	-
247	--	--	-	--	-
248	3.468 + 5	--	-	--	-
249	1.341 + 5	--	-	--	-
250	4.505 + 5	--	-	--	-
251	2.308 + 6	0.24	23	0.10	23
252	8.875 + 5	0.025	33	--	-
253	2.983 + 6	0.060	23	0.074	24
254	1.018 + 6	--	-	--	-
255	3.916 + 5	--	-	--	-
256	1.316 + 6	--	-	--	-
257	3.479 + 6	0.015	51	--	-
258	1.338 + 6	--	-	--	-
259	4.497 + 6	--	-	--	-
260	4.187 + 5	--	-	--	-
261	1.610 + 5	--	-	--	-
262	5.412 + 5	--	-	--	-

TABLE D-II

CALCULATED REGION TOTALS, PHOEBUS 2A ABSORPTION RATES

Cell No.	Total Absorptions/sec-5000 MW Control Drum at 90°	Control Drum at 120°	Cell No.	Total Absorptions/sec-5000 MW Control Drum at 90°	Control Drum at 120°
1-63	1.193 + 20	1.194 + 20	68, 147-149	9.23 + 17	1.10 + 18
64-67	1.01 + 18	1.22 + 18	150-155	1.21 + 17	1.14 + 17
69-81	2.75 + 18	2.93 + 18	156-160	7.64 + 16	8.83 + 16
82-85	5.22 + 18	5.56 + 18	161-175	3.61 + 19	3.16 + 19
86-94	6.44 + 18	7.92 + 18	176-177	7.97 + 18	8.33 + 18
95-103	0	0	178-191	9.64 + 17	9.08 + 17
104-112	1.99 + 18	2.22 + 18	192-205	3.25 + 19	3.18 + 19
113-114	5.05 + 17	5.18 + 17	206-219	8.79 + 16	8.90 + 16
115-123	4.38 + 17	3.88 + 17	220-233	1.80 + 19	1.81 + 19
124-127	6.02 + 17	6.81 + 17	234-237	~ 0	~ 0
128-134	5.72 + 17	5.63 + 17	238-241	2.00 + 17	1.49 + 17
135-143	9.33 + 17	8.48 + 17	242-260	3.4 + 16	1.8 + 16
144-146	5.06 + 17	5.61 + 17	1-260	2.372 + 20	2.351 + 20

TABLE D-III

CALCULATED FISSION RATES FOR ~ 5000-MW PHOEBUS 2A

Cell No.	Control Drums at 90° 10^{-17} x Fissions/sec	Relative Error, %	Control Drums at 120° 10^{-17} x Fissions/sec	Relative Error, %	Cell No.	Control Drums at 90° 10^{-17} x Fissions/sec	Relative Error, %	Control Drums at 120° 10^{-17} x Fissions/sec	Relative Error, %
1	6.26	7	6.06	7	40	5.09	12	5.08	10
2	9.53	6	10.2	7	41	4.54	11	4.69	11
3	13.0	7	13.0	8	42	4.36	10	5.29	12
4	128	4	121	4	43	2.41	12	2.96	14
5	13.2	7	14.1	7	44	4.36	11	4.91	11
6	10.4	6	10.5	7	45	4.93	8	5.34	11
7	9.18	6	8.18	6	46	48.4	4	54.5	4
8	8.85	6	8.66	5	47	4.94	12	6.33	10
9	13.9	5	13.7	6	48	4.53	11	4.45	10
10	20.0	6	17.5	6	49	2.13	14	3.28	12
11	171	4	175	3	50	2.75	15	2.99	15
12	18.5	7	19.4	7	51	3.15	12	3.54	12
13	14.9	6	14.5	5	52	6.13	10	5.13	10
14	13.5	5	12.3	5	53	44.9	4	54.3	4
15	10.7	6	10.9	6	54	5.65	11	6.26	11
16	19.8	6	17.3	5	55	3.79	14	5.34	11
17	23.6	7	19.0	6	56	2.76	11	3.28	11
18	240	3	216	3	57	1.38	17	1.84	19
19	24.0	7	26.8	8	58	1.87	16	2.70	15
20	18.9	6	19.7	6	59	2.53	14	3.28	11
21	15.2	5	15.1	5	60	29.2	5	32.3	5
22	17.4	6	16.5	6	61	3.45	14	4.21	12
23	28.0	6	26.3	3	62	2.70	16	2.64	13
24	33.8	7	33.5	7	63	1.71	15	1.74	14
25	328	4	333	3	1-7	189.6		183.0	
26	33.5	8	37.6	7	8-14	260.7		261.1	
27	27.0	6	32.1	6	15-21	352.2		324.8	
28	21.6	6	26.0	6	22-28	489.3		505.0	
29	3.15	13	2.67	12	29-35	80.8		90.4	
30	4.66	11	4.93	9	36-42	78.7		80.4	
31	5.29	9	6.24	10	43-49	71.7		81.8	
32	52.7	4	59.6	5	50-56	69.1		80.8	
33	6.41	10	7.31	10	57-63	42.8		48.7	
34	4.84	11	4.93	10	1-63	1635		1656	
35	3.74	11	4.72	13					
36	2.66	15	2.58	14					
37	3.77	12	3.47	10					
38	4.81	9	5.53	9					
39	53.5	4	53.8	4					

KT/db: 278 (50)